Experimental study on the flexural behavior of ECC-concrete hybrid composite beams reinforced with FRP and steel bars

Wen-Jie Ge[1*], Ashraf F. Ashour[2], Jiamin Yu[3], Peiqi Gao[4], Da-Fu Cao[5], Chen Cai[6], Xiang Ji[7]

(1. Ph.D., Associate Professor, College of Civil Science and Engineering, Yangzhou University, Yangzhou 225127, China(corresponding author), E-mail: gewj@yzu.edu.cn; 2. Ph.D., Professor, School of Engineering, University of Bradford, Bradford, BD7 1DP, UK; 3. M.S. Candidate, College of Civil Science and Engineering, Yangzhou University, Yangzhou 225127, China; 4. M.S. Candidate, College of Civil Science and Engineering, Yangzhou University, Yangzhou 225127, China; 5. M.S., Professor, College of Civil Science and Engineering, Yangzhou University, Yangzhou 225127, China 6; M.S. Candidate, College of Civil Science and Engineering, Yangzhou University, Yangzhou 225127, China; 7. M.S. Candidate, College of Civil Science and Engineering, Yangzhou University, Yangzhou 225127, China.)

Abstract: This paper aims to investigate the flexural behavior of engineered cementitious composite (ECC)-concrete hybrid composite beams reinforced with fiber reinforced polymer (FRP) bars and steel bars. Thirty two hybrid reinforced composite beams having various ECC height replacement ratio and combinations of FRP and steel reinforcements were experimentally tested to failure in flexure. Test results showed that cracking, yield and ultimate moments as well as the stiffness of hybrid and ECC beams are improved compared with traditional concrete beams having the same reinforcement, owing to the excellent tensile properties of ECC materials. The average crack spacing and width decrease with the increase of ECC height replacement ratio. The ductility of hybrid reinforced composite beams is higher than that of traditional reinforced concrete beams while their practical reinforcement ratios are similar. Reinforced ECC beams show considerable energy dissipation capacity owing to ECC's excellent deformation ability. Considering the constitutive models of materials, compatibility and equilibrium conditions, formulas for the prediction of cracking, yield and ultimate moments as well as deflections of hybrid reinforced ECC-concrete composite beams are developed. The proposed formulas are in good agreement with the experimental results. A comprehensive parametric analysis is, then, conducted to illustrate the effect of reinforcement, ECC and concrete properties on the moment capacity, curvature, ductility and energy dissipation of composite beams.

Keywords: ECC; concrete; composite beams; hybrid reinforcement; flexural behavior; steel bars; FRP bars.

Introduction

Many reinforced concrete structures, for example bridges, dams and off-shore structures, are exposed to de-icing salts, combinations of temperature, moisture and chlorides, causing corrosion of steel reinforcement. They, consequently, deteriorate and cannot meet the requirement of ultimate limit state and durability. Over the last four decades, FRP materials are increasingly used as a substitute to steel reinforcement in concrete structures (Masmoudi et al.1998; Grace et al. 1999; Pecce et al. 2000; Aiello et al. 2000; Gravina et al. 2008; Tu et al. 2009; Soric et al. 2010) for the advantages of high strength and anti-erosion properties. But FRP reinforcement has the properties of low elastic modulus and linear deformation until rupture, leading to large deflections, crack widths and brittle failure, which have been obstructing FRP structures from being widely used in civil engineering.

In order to enhance both ductility and durability of concrete structures, some researchers (Aiello et al. 2002; Leung et al. 2003; Qu et al. 2009; Lau et al.2010; Kara et al. 2015; Ge et al. 2015) proposed hybrid steel and FRP reinforcement, where FRP reinforcement is located at the corners of concrete elements and steel bars are placed inside providing more corrosion protection. The excellent crack control ability and durability of ECC material has encouraged the use of ECC in the tensile zone around the longitudinal steel reinforcement (Maalej et al. 1995; Wang et al.2001; Yuan et al. 2014). The results showed that the flexural capacity and deformation ability have slightly improved, but the crack width before yielding of steel reinforcement has significantly reduced to be just 20% of that in conventional reinforced concrete beams (Zhang et al. 2006; Xu et al. 2009; Xu et al. 2010; Zhang et al. 2010; Maalej et al.2012; Xu et al. 2013; Ge et al. 2018). On the other hand, ECC beams (Cai et al. 2017) and ECC-concrete composite beams (Maalej et al.2005; Yuan et al. 2013) reinforced with FRP bars were also studied to solve cracking and deflection problems associated with brittleness of FRP reinforced beams.

In this paper, a more effective system, combining ECC and concrete as the main body of structural beams reinforced with hybrid steel and FRP bars is proposed. A comprehensive experimental investigation of hybrid composite reinforced concrete beams having various ECC height replacement ratio and reinforcement index is conducted and presented in this paper. An analytical technique is proposed for predicting the cracking, yield and ultimate moments as well as the failure modes and deflection response throughout the loading. The technique is based on realistic constitutive models of materials, compatibility of strains and equilibrium of forces. A detailed parametric study is, then, carried out to establish the variation of flexural behavior of composite beams with the main influential parameters. Simplified equations are also proposed for the ultimate moments for each mode of failure.

Experimental program

Test specimens design

In total, thirty two beam specimens were tested to examine the behavior of the proposed hybrid reinforced composite concrete system as well as validating the developed analytical analysis presented later in this paper. The test specimens were divided into eight groups according to the amount and combination of steel and FRP reinforcement, while each group comprised of four specimens with different ECC height replacement ratio r_h (defined as the ECC thickness in tension zone h_e to effective height of cross-section h_0, $r_h = h_e / h_0$). Test specimen reinforcement and ECC height replacement ratio are shown in table 1 and schematic diagram of specimens is shown in figure 1. In each group, four ECC height replacement ratio was selected, namely r_h = 0.00, 0.29, 0.57 and 1.14, where r_h = 0.00 and 1.14 indicate fully traditional concrete and fully ECC beam specimens, respectively. The cross-section width b and cross-section height h are 150 mm and 200 mm, respectively; specimen length l, pure flexural length l_m, flexural-shear length l_{mv} and free overhang length l_f are 1500 mm, 400 mm, 500 mm and 50 mm, respectively; cross-section effective height h_0 is 175 mm, the distance of the center of steel bars and the concrete tensile edge h_s is 25mm; A_s and A_f are the cross-section areas of steel and FRP bars, respectively, ρ_s and ρ_f are the reinforcement ratio of steel and FRP bars ($\rho_s = A_s / (bh_0)$, $\rho_f = A_f / (bh_0)$), respectively, f_{fu} and f_y are the ultimate tensile strength of FRP bars and the yield strength of steel bars, respectively, E_f and E_s are the elastice modulous of FRP bars and steel bars, respectively, ρ_h (= $\rho_s + \rho_f$), $\rho_{h,f}$ (= $\rho_s + \rho_f f_{fu} / f_y$) and $\rho_{h,E}$ (= $\rho_s + \rho_f E_f / E_s$) represent the practical reinforcement ratio, nominal reinforcement ratio using strength conversion ratio (f_{fu} / f_y) and nominal reinforcement ratio using elastic modulus conversion ratio (E_f / E_s), respectively, A_{sv} and A_s' represent the stirrup and erection bars, respectively.

Table 1 Test specimen reinforcement and ECC height replacement ratio

Beam notation	A_s	A_f	ρ_h (%)	$\rho_{h,f}$ (%)	$\rho_{h,E}$ (%)	A_{sv}	A_s'	r_h
HB	2Φ12	—	0.86	0.86	0.86	Φ8@100	2Φ10	0.00/0.29/0.57/1.14
HC	2Φ12	Φ8	1.05	1.56	0.91	Φ8@100	2Φ10	0.00/0.29/0.57/1.14
HD	1Φ10	2Φ8	0.68	1.47	0.39	Φ8@100	2Φ10	0.00/0.29/0.57/1.14
HE	1Φ12	2Φ8	0.81	1.60	0.53	Φ8@100	2Φ10	0.00/0.29/0.57/1.14
HF	2Φ10	Φ8	0.79	1.19	0.65	Φ8@100	2Φ10	0.00/0.29/0.57/1.14
HG	2Φ12	Φ8	1.05	1.45	0.91	Φ8@100	2Φ10	0.00/0.29/0.57/1.14
HH	2Φ12	Φ8	1.05	1.33	0.91	Φ8@62.5	2Φ10	0.00/0.29/0.57/1.14
HK	—	3Φ8	0.57	1.76	0.14	Φ8@100	2Φ10	0.00/0.29/0.57/1.14

Note: Φ, HRB335 grade steel bar; Φ, HRB400 grade steel bar; Φ, HRB500 steel bar; Φ, FRP bar.

Displacement trancedusers were used to measure the deflections at the support points, loading points and mid-span. Strain gauges were also arranged along the height of the beam cross-section to measure the strains in ECC/concrete. An oil hydraulic jack was used to load each specimen through a steel beam spreader to achieve the two point loading system shown in figure 1.

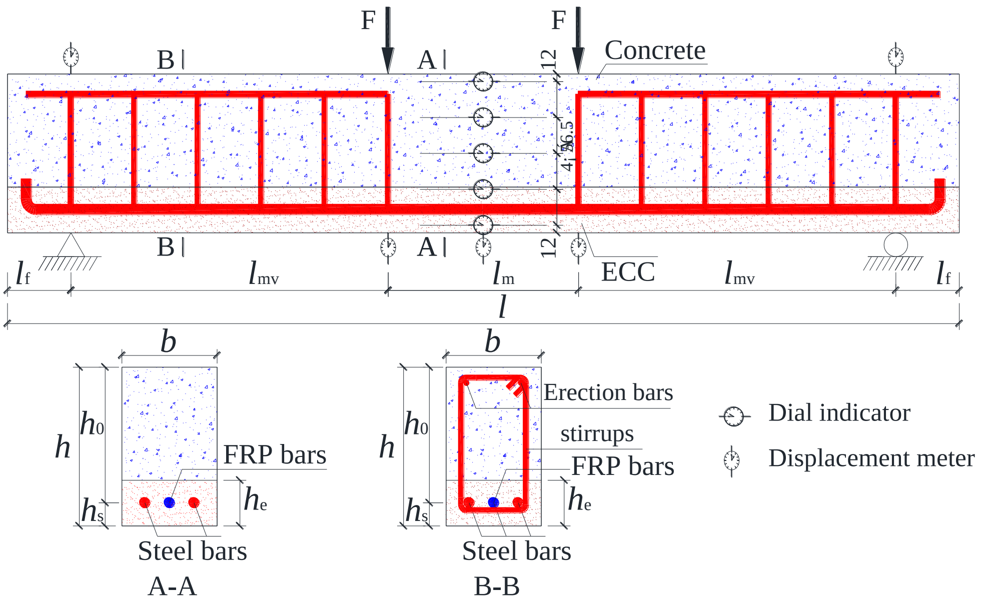

Fig.1 Schematic diagram of hybrid reinforced ECC-concrete composite beams

Materials

Portland cement, grade I fly ash, superfine silica fume, 100-200 mesh special fine quartz sand, sika poly acid water reducer and RECS15*12 type polyvinyl alcohol (PVA) fiber were used for producing ECC. The mass ratio of cement, fly ash, silica fume, sand and water were 1.0 : 3.0 : 1.0 : 0.36 : 0.3, and the fiber volume fraction is 2.0 %. Figure 2 presents the tensile stress-strain curves of ECC used, obtained from testing three rectangular flat-plates with a size of 160 mm × 40 mm × 15 mm in tension. The tensile stress at first cracking f_{etc} = 2.0 MPa, ultimate tensile strength f_{tu} = 2.4 MPa, tensile elastic modulus E_e = 8.2 GPa, tensile strain at first cracking ε_{etc} = 0.23 × 10^{-3} and ultimate tensile strain ε_{etu} = 0.025. On the other hand, three prismatic specimens with a size of 40 mm × 40 mm ×160mm were made for compressive tests and the compressive stress-strain of ECC are shown in figure 3. The peak compressive stress of ECC f_{ecp} = 31.4 MPa and its corresponding strain ε_{ecp} = 0.0036.

(a) Test

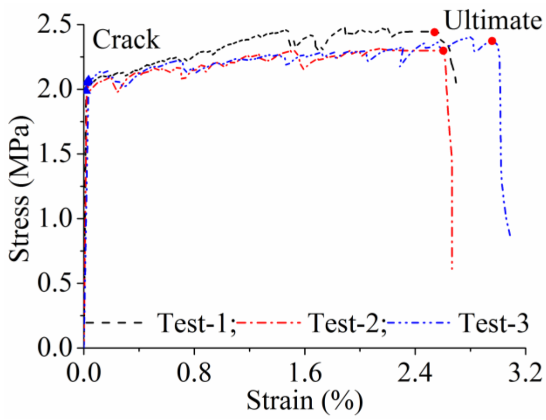

(b) Stress-strain curves

Fig.2 Tensile test of ECC

(a) Test

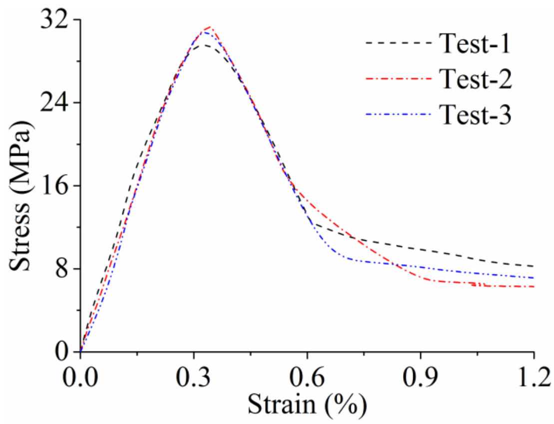

(b) Stress-strain curves

Fig.3 Compressive test of ECC

The mechanical properties of steel bars were measured as listed in table 2 and figure 4, where f_y, f_u and E are the yield strength, ultimate strength and elastic modulus of reinforcing steel bars, respectively.

Table 2 Mechanical properties of reinforcing bars

Bar type	Diameter (mm)	f_y (MPa)	f_u (MPa)	E (GPa)
HRB335	12	340	460	199
HRB400	8	406	485	198
HRB400	10	403	495	198
HRB400	12	408	503	199
HRB500	12	507	630	199
BFRP	8	—	1250	50

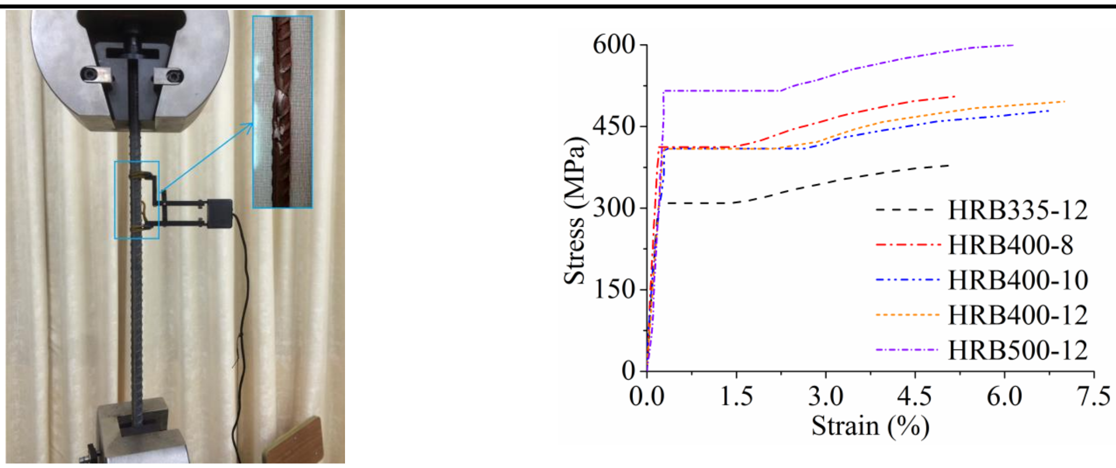

(a) Test (b) Stress-strain curves

Fig.4 Tensile test of steel reinforcement

The mechanical properties of basalt fiber reinforced polymer (BFRP) bars was obtained from testing three specimens according to ACI 440.3R-04(ACI 2004) as shown in figure 5(a); the total length of the specimen was 1200 mm and the free length was 400 mm. The stress-strain curves are shown in figure 5(b) and its tensile prosperities are shown in table 2.

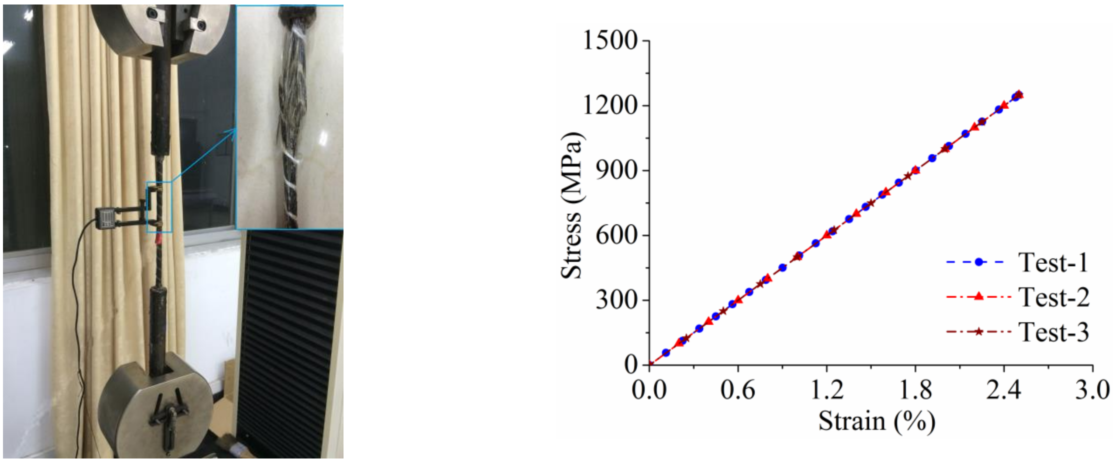

(a) Test (b) Stress-strain curves

Fig.5 Tensile test of FRP rebar

Three cube specimens with a size of 150 mm × 150 mm ×150mm were made for concrete mechanical properties tests (Chinese National Standard 2002; Chinese National Standard 2010). Compressive strength f_c = 30.16 MPa, tensile strength f_t = 2.55 MPa and ultimate tensile strain ε_{tu} = 110×10^{-6}.

Experimental results

Strain distribution along the height of cross-section

Average ECC/concrete strain distributions along the height of cross-section (group HG) for various acting moments are shown in figure 6. Other groups exhibited similar strain distribution, therefore not presented here.

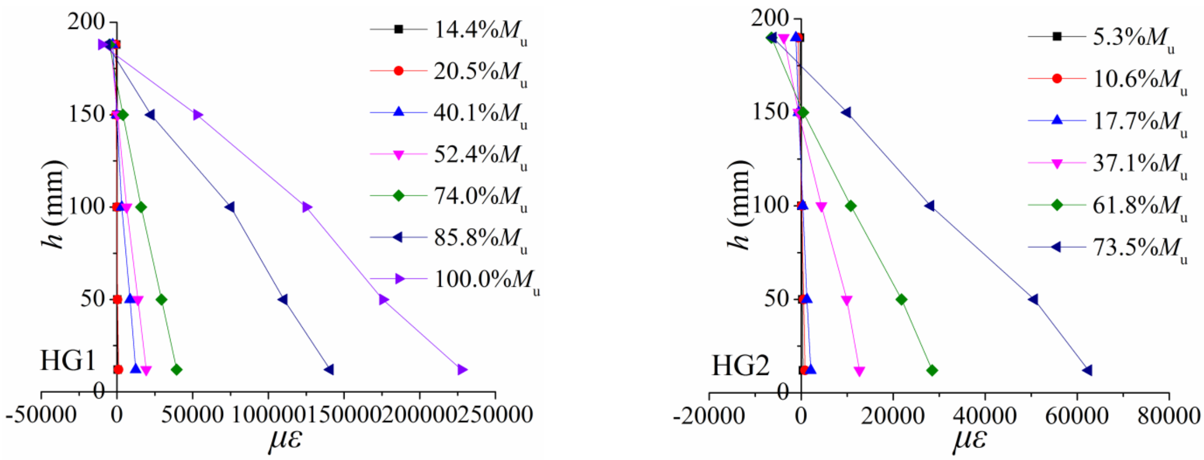

(a) HG1 (b) HG2

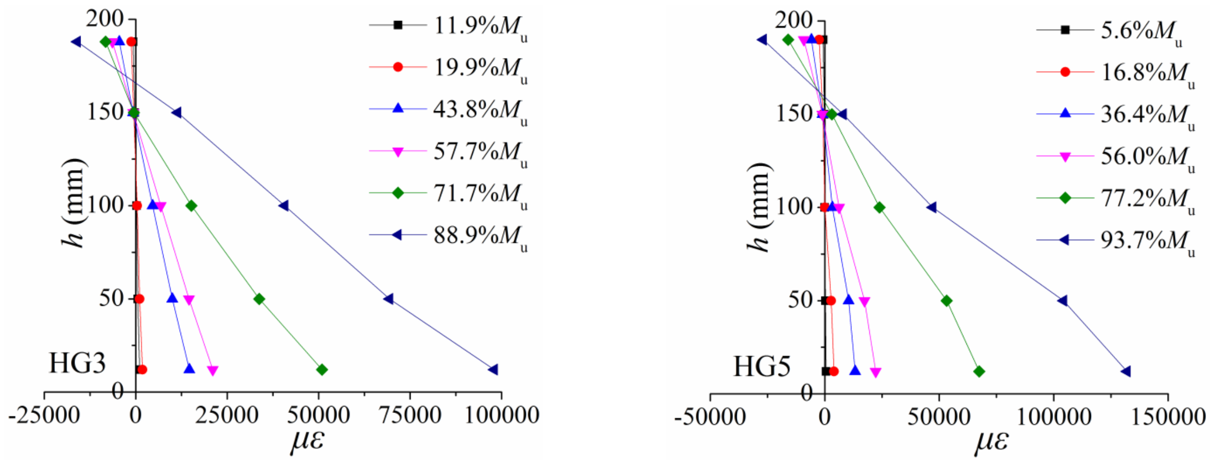

(c) HG3 (d) HG5

Fig.6 Average strain distribution along the height of cross-section

Figure 6 shows that the strain distribution is almost linear, indicating that:

- The validity of the assumption that plane section perpendicular to the axis of the beam remains plane after loading;
- No delamination between ECC and concrete at various stages of loading in this investigation.

Loading-deflection curves

For the hybrid reinforced ECC beams, tiny cracks were first observed in the pure bending region as the load increased. After that, the slope of the load-deflection curve showed a slight drop and new flexural cracks were formed in the beam with the increase of loading. For beams having steel reinforcement, yielding of such reinforcement was reached, followed by a quick increase in the mid-span deflection and crack width with little increase of the applied load. With further increase of loading, the outermost fiber of concrete in the compression zone reached the ultimate strain and crushed, indicating a compressive failure mode. The crack patterns and failure modes at failure of specimens HE1, HE2, HE3 and HE5 are shown in figure 7.

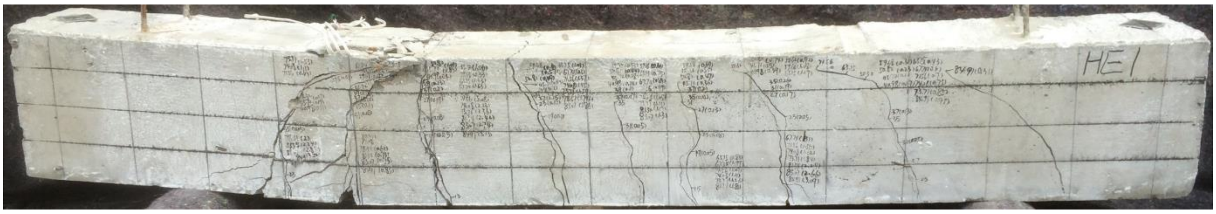

(a) HE1

(b) HE2

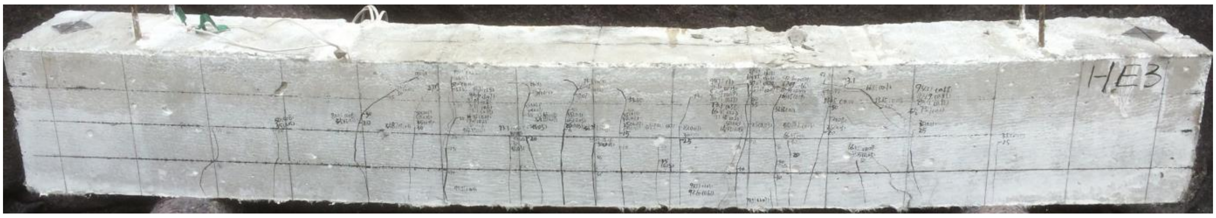

(c) HE3

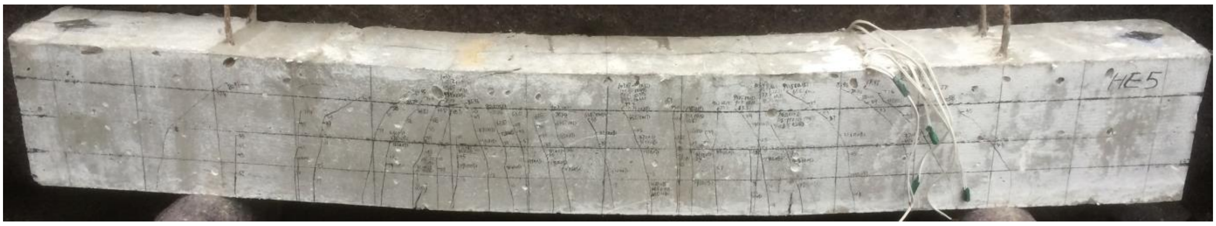

(d) HE5

Fig.7 Crack patterns and failure modes of group HE

The mid-span moment-deflection (M-f) curves of groups HB, HE, HF and HK are shown in figure 8. The mid-span deflection f can be obtained by subtracting the average settlement value of the two bearing points with the measured deformation of mid-span, whereas the moment M can be obtained by multiplying the measured load F by flexural-shear length l_{mv} (as shown in figure 1).

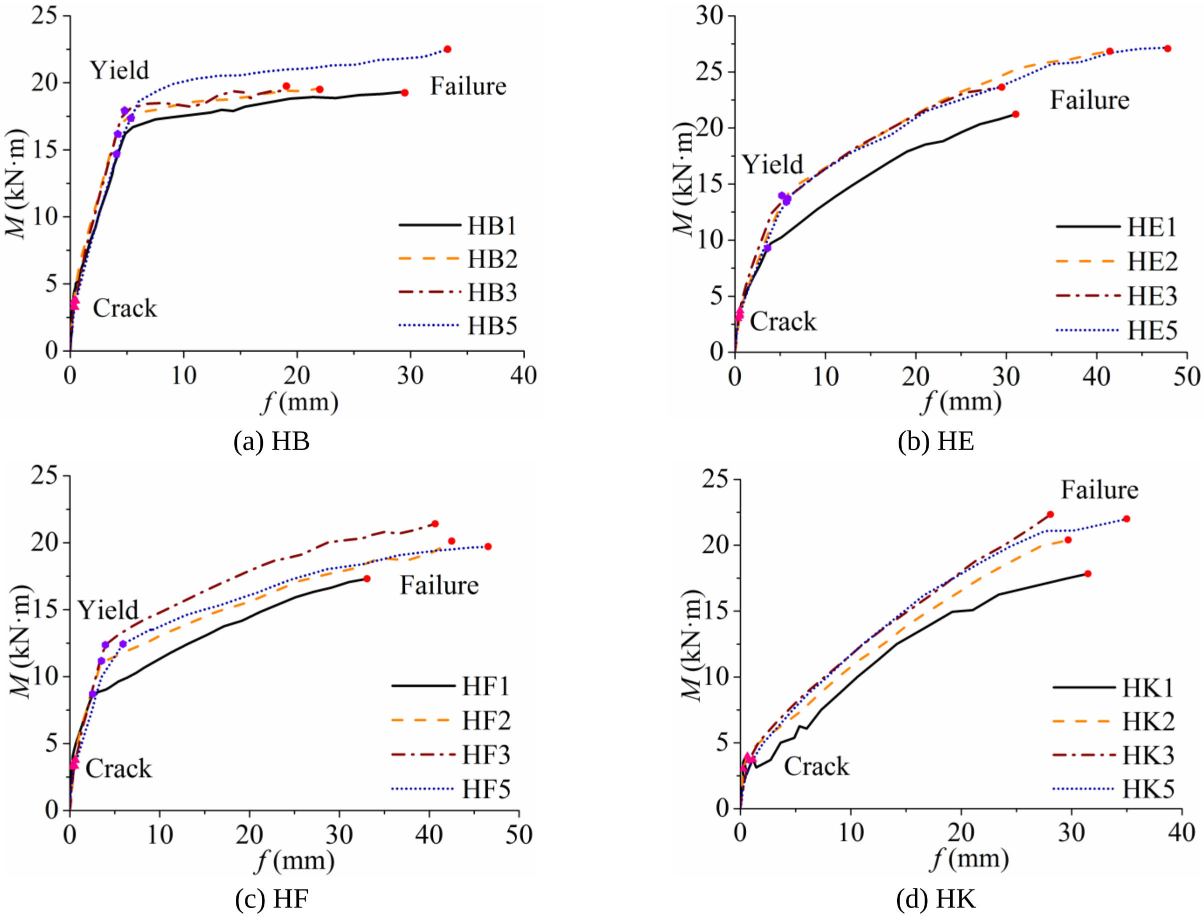

(a) HB (b) HE

(c) HF (d) HK

Fig.8 Comparison of moment-deflection curves

As can be observed from figures 7 and 8, no delamination between concrete and ECC layer was detected until failure. At the same applied load, the deflection of composite beams and ECC beams are less than that of concrete beams, regardless of the reinforcement used, indicating that higher stiffness can be obtained when ECC is used. The loading process of steel reinforced beams and hybrid reinforced beams can be divided into three stages: 1). from being loaded to the cracking of concrete/ECC; 2). from cracking to yielding of steel reinforcement and 3) from yielding of steel reinforcement to failure. After yielding of steel bars, the deflections of the steel reinforced beams continually increased even the load does not increase while deflections of hybrid reinforced beams increased with the increase of loading. On the other hand, the loading process of FRP reinforced beams can be divided into two stages: 1). from being loaded to the cracking of concrete/ECC and 2).

from cracking to failure of beams.

Cracking, yield and ultimate moment

Cracking, yield, ultimate moments and corresponding deflections of specimens are shown in table 3.

Table 3 Experimental values of cracking, yield and ultimate moments and corresponding deflections

Beam notation	ρ_h (%)	$\rho_{h,f}$ (%)	$\rho_{h,E}$ (%)	r_h	$M_{cr,e}$ (kN·m)	$d_{cr,e}$ (mm)	$M_{y,e}$ (kN·m)	$d_{y,e}$ (mm)	$M_{u,e}$ (kN·m)	$d_{u,e}$ (mm)
HB1	0.86	0.86	0.86	0.00	3.26	0.25	14.7	4.09	19.3	29.5
HB2				0.29	3.74	0.34	16.2	4.20	19.5	22.0
HB3				0.57	3.75	0.48	17.9	4.80	19.8	19.1
HB5				1.14	3.26	0.41	17.4	5.36	22.5	33.3
HC1	1.05	1.56	0.91	0.00	3.26	0.23	14.0	2.92	22.0	29.5
HC2				0.29	4.00	0.27	17.4	4.12	23.9	33.8
HC3				0.57	3.74	0.50	19.6	4.92	25.7	32.8
HC5				1.14	3.56	0.68	16.9	5.29	24.8	39.1
HD1	0.68	1.47	0.39	0.00	3.00	0.13	7.02	3.69	18.3	31.4
HD2				0.29	3.26	0.34	9.45	4.38	18.6	30.6
HD3				0.57	3.25	0.45	10.7	4.59	22.0	29.1
HD5				1.14	3.00	0.72	10.7	6.48	21.9	51.0
HE1	0.81	1.60	0.53	0.00	3.02	0.32	9.28	3.62	21.2	31.1
HE2				0.29	3.39	0.54	14.0	5.19	26.8	41.5
HE3				0.57	3.71	0.56	13.4	5.70	23.6	29.5
HE5				1.14	3.23	0.50	13.7	5.85	27.1	47.9
HF1	0.79	1.19	0.65	0.00	3.26	0.22	8.71	2.53	17.3	33.1
HF2				0.29	3.75	0.56	11.2	3.52	20.1	42.5
HF3				0.57	3.77	0.64	12.4	3.96	21.4	40.7
HF5				1.14	3.33	0.55	12.4	5.91	19.7	46.6
HG1	1.05	1.45	0.91	0.00	3.46	0.20	17.3	4.14	24.3	31.4
HG2				0.29	3.82	0.26	17.5	4.70	28.3	30.3
HG3				0.57	3.80	0.29	18.8	6.11	25.1	28.5
HG5				1.14	3.55	0.50	18.4	6.15	26.8	43.9
HH1	1.05	1.33	0.91	0.00	3.49	0.27	19.5	4.32	26.6	24.2
HH2				0.29	3.75	0.36	23.2	5.17	28.8	27.3
HH3				0.57	3.99	0.37	23.9	5.29	28.7	23.8
HH5				1.14	3.59	0.51	23.7	7.63	27.2	38.3
HK1	0.57	1.76	0.14	0.00	3.02	0.23	—	—	17.8	31.5
HK2				0.29	3.97	0.63	—	—	20.4	29.7
HK3				0.57	3.66	0.79	—	—	22.3	28.1
HK5				1.14	3.73	1.15	—	—	22.0	35.0

Note: $M_{cr,e}$, $M_{y,e}$ and $M_{u,e}$ are the experimental cracking, yield and ultimate moment, respectively, $d_{cr,e}$, $d_{y,e}$ and $d_{u,e}$ are the corresponding deflection of cracking, yield and ultimate moment, respectively.

As can be observed from table 3, the cracking, yield and ultimate moments of composite beams and ECC beams are higher than those of concrete beams, regardless of the reinforcement used. For specimens with the same nominal reinforcement ratio using elastic modulus conversion factor ($\rho_{h,E,HC}$ = $\rho_{h,E,HG}$ = $\rho_{h,E,HH}$ = 0.91 %), ultimate moment increases with the decrease of nominal reinforcement ratio using strength conversion factor ($\rho_{h,f,HC}$ = 1.38 % > $\rho_{h,f,HG}$ = 1.34 % > $\rho_{h,f,HH}$ = 1.24 %). For specimens with similar nominal reinforcement ratio converted by strength ratio ($\rho_{h,f,HC}$ = 1.56 % ≈ $\rho_{h,f,HE}$ = 1.60 %, $\rho_{h,f,HD}$ = 1.47 % ≈ $\rho_{h,f,HG}$ = 1.45 %), yield moment decreases with the decrease of nominal reinforcement ratio converted by elastic modulus ratio ($\rho_{h,E,HC}$ = 0.91 % > $\rho_{h,E,HE}$ = 0.53 %, $\rho_{h,E,HG}$ = 0.91 % > $\rho_{h,E,HD}$ = 0.39 %).

Cracks distribution and Failure mode

The moment-crack width (M-$\omega_{s,max}$) curves, number of cracks (n) and average crack spacing (l_{cr}) of groups HB, HE, HF and HK are shown in figure 9 and figure 10, respectively.

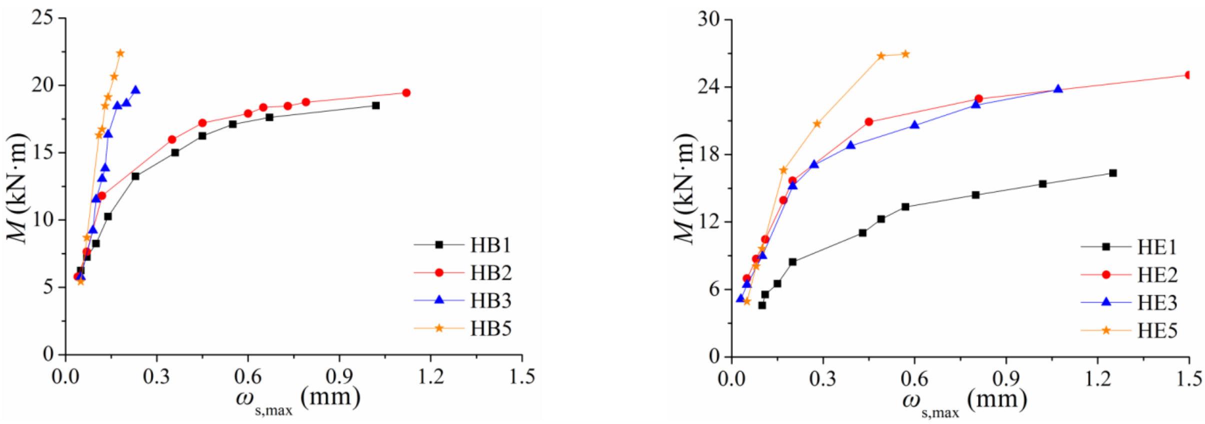

(a) HB (b) HE

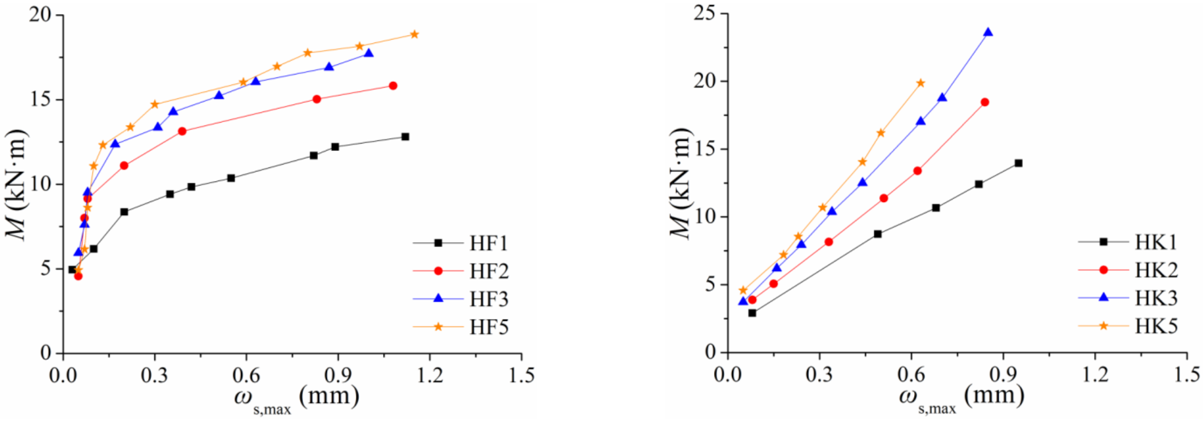

(c) HF (d) HK

Fig.9 Comparison of load-crack width curves

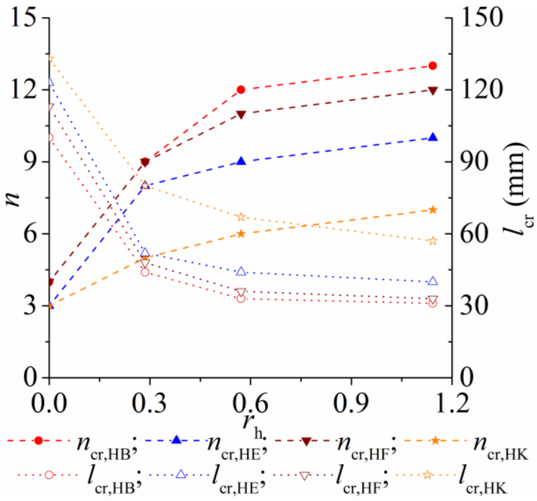

Fig.10 Number of cracks and average crack pacing of groups HB, HE, HF and HK

As can be observed from figures 9 and 10, number of cracks increases while average crack spacing decreases with the increase of height replacement ratio. According to the experimental observation, the maximum crack width of specimens decrease with increasing the height replacement ratio, regardless of the reinforcement used. Taking group HF as example, under the same moment of 12.0 kN·m, the maximum crack width of specimens HF1, HF2, HF3 and HF5 are 0.86 mm, 0.28 mm, 0.16 mm and 0.12 mm, respectively.

Ductility and energy dissipation

Ductility and energy dissipation of specimens are shown in table 4, u_d is the deflection ductility defined as the ultimate deflection d_u to yield deflection d_y, $u_d = d_u / d_y$, E_d is the energy dissipation (in

N·m^2) defined by the including area of the moment-deflection (M-d) curves, for steel reinforced beams and hybrid reinforced beams, $E_d = M_{cr}\, d_{cr} / 2 + (M_{cr} + M_y)\,(d_y - d_{cr}) / 2 + (M_y + M_u)\,(d_u - d_y) / 2$, for FRP reinforced beams, $E_d = M_{cr}\, d_{cr} / 2 + (M_{cr} + M_u)\,(d_u - d_{cr}) / 2$.

Table 4 Ductility and energy dissipation of specimens

Beam notation	ρ_h (%)	$\rho_{h,f}$ (%)	$\rho_{h,E}$ (%)	r_h	u_d	E_d (N·m^2)
HB1	0.86	0.86	0.86	0.00	7.21	466
HB2				0.29	5.24	357
HB3				0.57	3.97	316
HB5				1.14	6.21	608
HC1	1.05	1.56	0.91	0.00	10.1	502
HC2				0.29	8.21	655
HC3				0.57	6.66	684
HC5				1.14	7.38	752
HD1	0.68	1.47	0.39	0.00	8.50	369
HD2				0.29	6.99	395
HD3				0.57	6.33	429
HD5				1.14	7.87	767
HE1	0.81	1.60	0.53	0.00	8.58	439
HE2				0.29	7.99	781
HE3				0.57	5.18	486
HE5				1.14	8.18	903
HF1	0.79	1.19	0.65	0.00	13.1	412
HF2				0.29	12.1	633
HF3				0.57	10.3	648
HF5				1.14	7.87	696
HG1	1.05	1.45	0.91	0.00	7.58	608
HG2				0.29	6.46	635
HG3				0.57	4.66	558
HG5				1.14	7.14	917
HH1	1.05	1.33	0.91	0.00	5.61	507
HH2				0.29	5.27	641
HH3				0.57	4.50	556
HH5				1.14	5.03	880
HK1	0.57	1.76	0.14	0.00	—	326
HK2				0.29	—	355
HK3				0.57	—	356
HK5				1.14	—	438

As can be observed from table 4, the ductility of composite beams is less than that of concrete beams as ECC can provide tensile stress until failure, but the energy dissipation of reinforced ECC beams is higher than that of reinforced concrete beams and composite beams as the ultimate compressive strain of ECC is higher than that of concrete. For composite beams, ductility decreases with the increase of ECC height replacement ratio. For specimens with similar practical reinforcement ratio ($\rho_{\mathrm{h,\,HB}}$ = 0.86 % ≈ $\rho_{\mathrm{h,\,HE}}$ = 0.81 %), ductility of hybrid reinforced beams are higher than that of reinforced concrete beams. For specimens with the same nominal reinforcement ratio converted by elastic modulus ($\rho_{\mathrm{h,E,HC}}$ = $\rho_{\mathrm{h,E,HG}}$ = $\rho_{\mathrm{h,E,HH}}$ = 0.91 %), ductility increases with the increase of nominal reinforcement ratio converted by strength. Energy dissipation of steel reinforced beams and hybrid reinforced beams are higher than that of FRP reinforced beams.

Materials constitutive model

Reinforcement

The constitutive relationships of steel bars and FRP bars are shown in figure 11, where σ and ε are the stress and strain in materials, respectively; f_{sy}, E_{s}, $\varepsilon_{\mathrm{sy}}$ and $\varepsilon_{\mathrm{su}}$ are the yield strength, elastic modulus, yield strain and ultimate tensile strain (assumed to be 0.01) of steel bars, respectively; f_{fu}, E_{f} and $\varepsilon_{\mathrm{fu}}$ are the tensile strength, elastic modulus and ultimate tensile strain of FRP bars, respectively.

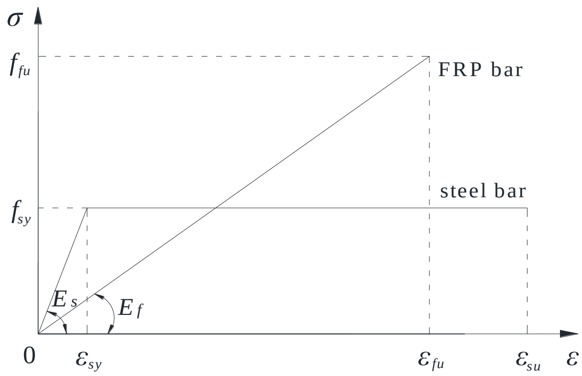

Fig.11 Constitutive relationships of steel bar

Concrete

The compressive stress-strain curve of concrete (Chinese National Standard 2010) is shown in figure 12(a) and can be expressed by:

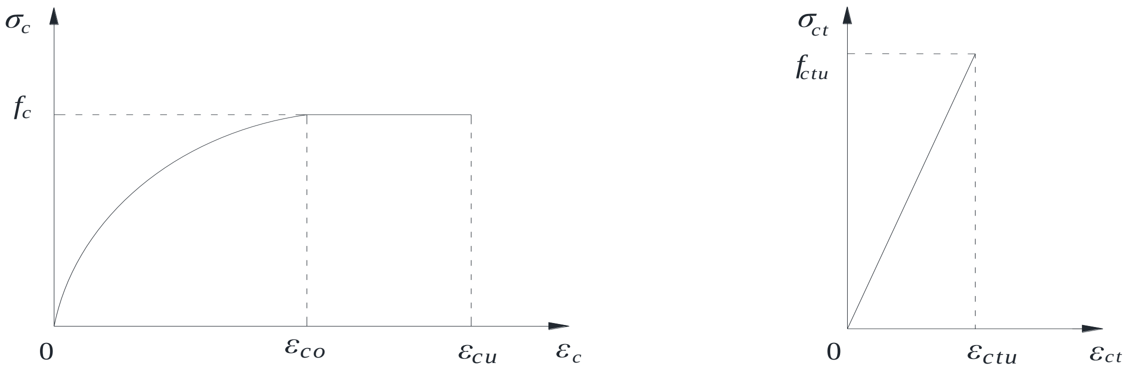

(a) Compression (b) Tension

Fig.12 Constitutive relationships of concrete

$$\sigma_{\mathrm{c}} = \begin{cases} f_{\mathrm{c}}\left[1-\left(1-\varepsilon_{\mathrm{c}}/\varepsilon_{\mathrm{co}}\right)^{\mathrm{n}}\right] & ,0 \le \varepsilon_{\mathrm{c}} \le \varepsilon_{\mathrm{co}} \\ f_{\mathrm{c}} & ,\varepsilon_{\mathrm{co}} < \varepsilon_{\mathrm{c}} \le \varepsilon_{\mathrm{cu}} \end{cases} \tag{1}$$

$$n = 2-\left(f_{\mathrm{cu,k}}-50\right)/60 \tag{2}$$

$$\varepsilon_{\mathrm{co}} = 0.002+0.5\left(f_{\mathrm{cu,k}}-50\right)\times 10^{-5} \tag{3}$$

$$\varepsilon_{\mathrm{cu}} = 0.0033-0.5\left(f_{\mathrm{cu,k}}-50\right)\times 10^{-5} \tag{4}$$

where ε_{c} and σ_{c} are the compressive strain and stress in concrete, f_{c} is the concrete compressive strength (in MPa), $\varepsilon_{\mathrm{co}}$ (≥ 0.002) is the compressive strain corresponding to concrete stress of f_{c}, $\varepsilon_{\mathrm{cu}}$ (≤ 0.0033) is the ultimate compressive strain of concrete, $f_{\mathrm{cu,k}}$ is the concrete cube compressive strength (in MPa) and n is a coefficient related to compressive strength of concrete (≤ 2.0).

The concrete uniaxial tensile stress-strain model is shown in figure 12(b) and can be represented by the following equation,

ε

$$\sigma_{\mathrm{ct}}=\begin{cases} f_{\mathrm{ctu}}\,\varepsilon_{\mathrm{ct}}/\varepsilon_{\mathrm{ctu}} & ,0\le\varepsilon_{\mathrm{ct}}\le\varepsilon_{\mathrm{ctu}} \\ 0 & ,\varepsilon_{\mathrm{ct}}>\varepsilon_{\mathrm{ctu}} \end{cases} \tag{5}$$

where $\varepsilon_{\mathrm{ct}}$ and σ_{ct} are the tensile strain and stress in concrete, f_{ctu} and $\varepsilon_{\mathrm{ctu}}$ are the ultimate uniaxial tensile stress and corresponding strain.

ECC

The compressive stress-strain curve (Yuan et al. 2013) of ECC is shown in figure 13(a) and can be formulated by:

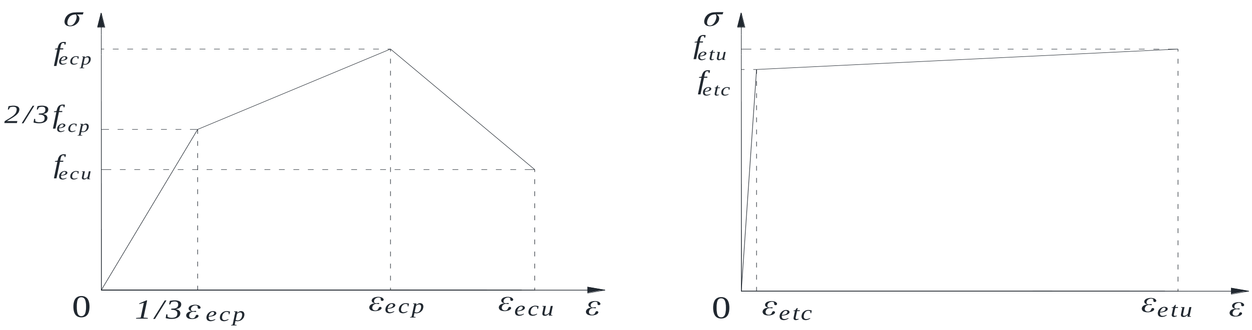

(a) Compression (b) Tension

Fig.13 Constitutive relationships of ECC

$$\sigma_{\mathrm{ec}}=\begin{cases} 2f_{\mathrm{ecp}}\varepsilon_{\mathrm{ec}}/\varepsilon_{\mathrm{ecp}} & ,0\le\varepsilon_{\mathrm{ec}}\le\varepsilon_{\mathrm{ecp}}/3 \\ f_{\mathrm{ecp}}/2+f_{\mathrm{ecp}}\varepsilon_{\mathrm{ec}}/(2\varepsilon_{\mathrm{ecp}}) & ,\varepsilon_{\mathrm{ecp}}/3<\varepsilon_{\mathrm{ec}}\le\varepsilon_{\mathrm{ecp}} \\ 2f_{\mathrm{ecp}}-f_{\mathrm{ecp}}\varepsilon_{\mathrm{ec}}/\varepsilon_{\mathrm{ecp}} & ,\varepsilon_{\mathrm{ecp}}<\varepsilon_{\mathrm{ec}}\le\varepsilon_{\mathrm{ecu}} \end{cases} \tag{6}$$

where $\varepsilon_{\mathrm{ec}}$ and σ_{ec} are the compressive strain and stress in ECC, f_{ecp} is the compressive strength of ECC (peak point of the curve), $\varepsilon_{\mathrm{ecp}}$ is the compressive strain corresponding to peak stress f_{ecp}, f_{ecu} is the ultimate compressive stress (after peak point) and $\varepsilon_{\mathrm{ecu}}$ is the ultimate compressive strain corresponding to ultimate stress f_{ecu}. In this paper, it is assumed that $f_{\mathrm{ecu}} = 0.5\, f_{\mathrm{ecp}}$ and $\varepsilon_{\mathrm{ecu}} = 1.5\, \varepsilon_{\mathrm{ecp}}$ (Yuan et al. 2013).

The tensile stress-strain curve (Maalej et al. 1995) of ECC is shown in figure 13(b) and can be expressed by the following equation,

$$\sigma_{\mathrm{et}}=\begin{cases} f_{\mathrm{etc}}\varepsilon_{\mathrm{et}}/\varepsilon_{\mathrm{etc}} & ,0\le\varepsilon_{\mathrm{et}}\le\varepsilon_{\mathrm{etc}} \\ f_{\mathrm{etc}}+\left(f_{\mathrm{etu}}-f_{\mathrm{etc}}\right)\left(\varepsilon_{\mathrm{et}}-\varepsilon_{\mathrm{etc}}\right)/\left(\varepsilon_{\mathrm{etu}}-\varepsilon_{\mathrm{etc}}\right) & ,\varepsilon_{\mathrm{etc}}<\varepsilon_{\mathrm{et}}\le\varepsilon_{\mathrm{etu}} \end{cases} \tag{7}$$

where $\varepsilon_{\mathrm{et}}$ and σ_{et} are the tensile strain and stress in ECC, f_{etc} and $\varepsilon_{\mathrm{etc}}$ are the tensile strength and corresponding strain at first cracking, f_{etu} and $\varepsilon_{\mathrm{etu}}$ are the ultimate tensile strength and corresponding strain.

Cracking and failure mode

Cracking modes

The cross-section strain distribution of ECC-concrete beams is shown in figure 14, where *b* is the width of cross-section, *h* is the height of cross-section, h_{s} is the distance of the core of steel/FRP bars to the cross-section tensile edge, h_{e} is the thickness of ECC, h_{t} is the height of cross-section part in tension (neutral axis depth), $\varepsilon_{\mathrm{et}}$ is the maximum tensile strain in ECC, $\varepsilon_{\mathrm{ct}}$ is the maximum tensile strain in concrete, ε_{c} is the maximum compressive strain in concrete, ε_{s} and ε_{f} are the tensile strain in steel and FRP bars, respectively.

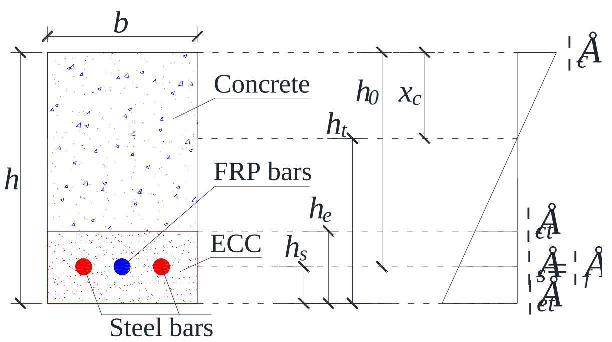

Fig.14 Cross-section strain distribution of elastic stage

If ECC and concrete simultaneously crack, the maximum ECC tensile strain $\varepsilon_{\mathrm{et}}$ = $\varepsilon_{\mathrm{etc}}$ and maximum concrete tensile strain $\varepsilon_{\mathrm{ct}}$ = $\varepsilon_{\mathrm{ctu}}$. According to the geometric similarity relationship, the following equation can be obtained,

$$\varepsilon_{\mathrm{ctu}}/\varepsilon_{\mathrm{etc}}=\left(h_{\mathrm{t}}-h_{\mathrm{e,b}}\right)/h_{\mathrm{t}} \tag{8}$$

where $h_{e,b}$ is the thickness of ECC that makes ECC and concrete incur cracking at the same time.

And then, the balance ECC thickness $h_{e,b}$ can be expressed as below:

$$h_{e,b} = \left(1 - \varepsilon_{ctu} / \varepsilon_{etc}\right) h_t \tag{9}$$

If $h_e < h_{e,b}$, concrete cracks before ECC, and when $h_e > h_{e,b}$, ECC incurs crack before concrete.

Failure Modes

According to the constitutive models of materials, failure modes of hybrid composite beams can be divided into three situations. The boundary state of failure modes is shown in figure 15, where ε_{hu} is the minimum ultimate tensile strain of steel and FRP bars, ε_{hu} = min (ε_{su}, ε_{fu}), x_c is the height of compressive zone.

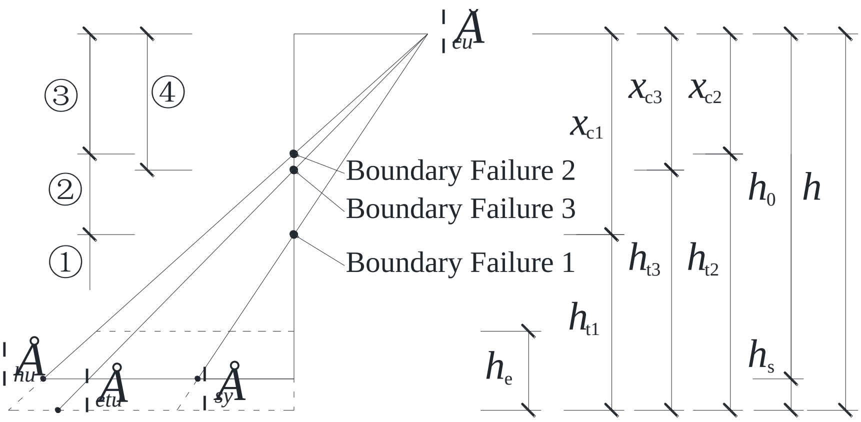

Fig.15 Cross-section strain distribution of boundary state

① $\varepsilon_c = \varepsilon_{cu}$, $\varepsilon_s = \varepsilon_f < \varepsilon_{sy}$

In this case, the steel bars do not yield, but the maximum compressive strain reaches the ultimate strain of concrete. This situation is similar to over-reinforced concrete beams and is not allowed in practical situations for its brittle failure.

② $\varepsilon_c = \varepsilon_{cu}$, $\varepsilon_{sy} < \varepsilon_s = \varepsilon_f \leq \varepsilon_{hu}$

The steel bars have yielded but its strain value does not reach the ultimate tensile strain of steel bars and FRP bars. However, the failure occurs when the concrete compressive strain reaches its ultimate strain. This situation is expected in practical structures for its ductile nature.

③ $\varepsilon_c < \varepsilon_{cu}$, $\varepsilon_{sy} < \varepsilon_s = \varepsilon_f = \varepsilon_{hu}$

The steel bars have yielded and its strain value reaches the ultimate tensile strain of steel bars and FRP bars. On the other hand, the compressive concrete strain does not reach the ultimate concrete compressive strain. This situation is not practically allowed as the amount of steel reinforcement is very small, allowing very large strains in steel.

④ $\varepsilon_c < \varepsilon_{cu}$, $\varepsilon_{sy} < \varepsilon_s = \varepsilon_f < \varepsilon_{hu}$, $\varepsilon_{et} = \varepsilon_{etu}$

The steel bars have yielded but its strain value does not reach the ultimate tensile strain of steel bars and FRP bars and the compressive concrete strain does not reach the ultimate concrete compressive strain. However, the failure occurs when the ECC tensile strain reaches its ultimate strain.

According to the force equilibrium of cross-section, the following equation can be obtained,

$$\int_0^{x_c} \sigma_c b dx = \sigma_s A_s + \sigma_f A_f + \int_0^{h_e} \sigma_{et} b dx \tag{10}$$

where x_c is the height of the compressive zone, $x_c = \varepsilon_{cu} h_0 / (\varepsilon_{cu} + \varepsilon_s)$.

Assuming the relative boundary compressive height $\xi_c = x_c / h_0$. The boundary relative neutral axis height ξ_{cb} can be defined according to the plane section assumption.

Boundary Failure 1:

$$\xi_{cb1} = \frac{x_{c1}}{h_0} = \frac{\varepsilon_{cu}}{\varepsilon_{cu} + \varepsilon_{sy}} \tag{11}$$

Boundary Failure 2:

$$\xi_{cb2} = \frac{x_{c2}}{h_0} = \frac{\varepsilon_{cu}}{\varepsilon_{cu} + \varepsilon_{hu}} \tag{12}$$

Boundary Failure 3:

$$\xi_{\mathrm{cb3}} = \frac{x_{\mathrm{c3}}}{h_0} = \frac{\varepsilon_{\mathrm{cu}}}{\varepsilon_{\mathrm{cu}} + \varepsilon_{\mathrm{etu}}} \tag{13}$$

For concrete grade less than C50 and considering tensile stress in ECC $\sigma_{\mathrm{et}} = f_{\mathrm{etc}}$ and $r_{\mathrm{h}} = h_{\mathrm{e}} / h_0$, Eq. (12) can be modified as below:

$$f_{\mathrm{c}} b h_0 \frac{\varepsilon_{\mathrm{cu}} - \varepsilon_{\mathrm{co}}/3}{\varepsilon_{\mathrm{cu}} + \varepsilon_{\mathrm{s}}} = \sigma_{\mathrm{s}} A_{\mathrm{s}} + \sigma_{\mathrm{f}} A_{\mathrm{f}} + f_{\mathrm{etc}} b h_{\mathrm{e}} \tag{14}$$

For Boundary Failure 1,

$$\rho_{\mathrm{s}} + \frac{E_{\mathrm{f}}}{E_{\mathrm{s}}} \rho_{\mathrm{f}} = \frac{f_{\mathrm{c}}}{f_{\mathrm{y}}} \cdot \frac{\varepsilon_{\mathrm{cu}} - \varepsilon_{\mathrm{co}}/3}{\varepsilon_{\mathrm{cu}} + \varepsilon_{\mathrm{sy}}} - r_{\mathrm{h}} \frac{f_{\mathrm{etc}}}{f_{\mathrm{y}}} \tag{15}$$

For Boundary Failure 2,

If $\varepsilon_{\mathrm{su}} < \varepsilon_{\mathrm{fu}}$.

$$\rho_{\mathrm{s}} + \frac{E_{\mathrm{f}}}{E_{\mathrm{s}}} \cdot \frac{\varepsilon_{\mathrm{su}}}{\varepsilon_{\mathrm{sy}}} \rho_{\mathrm{f}} = \frac{f_{\mathrm{c}}}{f_{\mathrm{y}}} \cdot \frac{\varepsilon_{\mathrm{cu}} - \varepsilon_{\mathrm{co}}/3}{\varepsilon_{\mathrm{cu}} + \varepsilon_{\mathrm{su}}} - r_{\mathrm{h}} \frac{f_{\mathrm{etc}}}{f_{\mathrm{y}}} \tag{16}$$

If $\varepsilon_{\mathrm{su}} \geq \varepsilon_{\mathrm{fu}}$.

$$\rho_{\mathrm{s}} + \frac{f_{\mathrm{fu}}}{f_{\mathrm{y}}} \rho_{\mathrm{f}} = \frac{f_{\mathrm{c}}}{f_{\mathrm{y}}} \cdot \frac{\varepsilon_{\mathrm{cu}} - \varepsilon_{\mathrm{co}}/3}{\varepsilon_{\mathrm{cu}} + \varepsilon_{\mathrm{fu}}} - r_{\mathrm{h}} \frac{f_{\mathrm{etc}}}{f_{\mathrm{y}}} \tag{17}$$

For Boundary Failure 3,

$$\rho_{\mathrm{s}} + \frac{E_{\mathrm{f}}}{f_{\mathrm{y}}} \cdot \frac{h_0 \varepsilon_{\mathrm{etu}} - h_{\mathrm{s}} \varepsilon_{\mathrm{cu}}}{h} \cdot \rho_{\mathrm{f}} = \frac{f_{\mathrm{c}}}{f_{\mathrm{y}}} \cdot \frac{h_0}{h} \cdot \frac{\varepsilon_{\mathrm{cu}} - \varepsilon_{\mathrm{co}}/3}{\varepsilon_{\mathrm{cu}} + \varepsilon_{\mathrm{etu}}} - r_{\mathrm{h}} \frac{f_{\mathrm{etc}}}{f_{\mathrm{y}}} \tag{18}$$

When maximum compressive concrete strain reaches the ultimate concrete compressive strain and ECC/longitudinal reinforcement reach their ultimate tensile strain simultaneously, the following equation can be obtained according to the plane section assumption.

$$\frac{\varepsilon_{\mathrm{cu}} + \varepsilon_{\mathrm{hu,b}}}{h_0} = \frac{\varepsilon_{\mathrm{cu}} + \varepsilon_{\mathrm{etu}}}{h} \tag{19}$$

Rearranging for $\varepsilon_{\mathrm{hu,b}}$:

$$\varepsilon_{\mathrm{hu,b}} = \frac{\varepsilon_{\mathrm{etu}} h_0 - \varepsilon_{\mathrm{cu}} h_{\mathrm{s}}}{h} \tag{20}$$

When $\varepsilon_{\mathrm{hu}} \leq \varepsilon_{\mathrm{hu,b}}$, longitudinal reinforcement reaches the ultimate tensile strain first, failure mode

① occurs for $\xi > \xi_{cb1}$, failure mode ② occurs for $\xi_{cb1} \le \xi \le \xi_{cb2}$ and failure mode ③ occurs for $\xi < \xi_{cb2}$. On the other hand, when $\varepsilon_{hu} > \varepsilon_{hu,b}$, ECC reinforcement reaches the ultimate tensile strain first, failure mode ① occurs for $\xi > \xi_{cb1}$, failure mode ② occurs for $\xi_{cb1} \le \xi \le \xi_{cb3}$ and failure mode ④ occurs for $\xi < \xi_{cb3}$. For this investigation, as $\varepsilon_{hu} = 0.0250 > \varepsilon_{hu,b} = 0.0215$, ECC reaches their ultimate tensile strain before longitudinal reinforcement.

So appropriate reinforcements should meet the following requirements simultaneously:

$$\rho_{\mathrm{s}} + \frac{E_{\mathrm{f}}}{f_{\mathrm{y}}} \cdot \frac{h_0 \varepsilon_{\mathrm{etu}} - h_{\mathrm{s}} \varepsilon_{\mathrm{cu}}}{h} \cdot \rho_{\mathrm{f}} \ge \frac{f_{\mathrm{c}}}{f_{\mathrm{y}}} \cdot \frac{h_0}{h} \cdot \frac{\varepsilon_{\mathrm{cu}} - \varepsilon_{\mathrm{co}}/3}{\varepsilon_{\mathrm{cu}} + \varepsilon_{\mathrm{etu}}} - r_{\mathrm{h}} \frac{f_{\mathrm{etc}}}{f_{\mathrm{y}}} \tag{21}$$

$$\rho_{\mathrm{h,E}} = \rho_{\mathrm{s}} + \frac{E_{\mathrm{f}}}{E_{\mathrm{s}}} \rho_{\mathrm{f}} \le \frac{f_{\mathrm{c}}}{f_{\mathrm{y}}} \cdot \frac{\varepsilon_{\mathrm{cu}} - \varepsilon_{\mathrm{co}}/3}{\varepsilon_{\mathrm{cu}} + \varepsilon_{\mathrm{sy}}} - r_{\mathrm{h}} \frac{f_{\mathrm{etc}}}{f_{\mathrm{y}}} \tag{22}$$

Cross-section analysis of composite beams

The following assumptions have been considered:

·The steel bars and concrete/ECC have perfect bond and no delamination between ECC and concrete is considered as observed in the experimental investigations presented above or others in the literature (Yuan et al. 2013).

·Each plane cross section perpendicular to the axis of the beam remains plane after loading.

·The whole loading process can be divided into three stages as observed in the experimental investigations:

1. Elastic stage (uncracked section): from being loaded to cracking (ECC or concrete).

2. Working stress stage: from cracking to yielding of steel bars.

3. Failure stage: from yielding of steel bars to the failure of composite beams (i.e. any material reaches its ultimate strain: (a). Compressive strain in concrete reaches ε_{cu}. (b). Tensile strain in ECC reaches ε_{etu}. (c). Tensile strain in steel bars reaches ε_{su}. (d). Tensile strain in FRP bars reaches ε_{fu}).

Cracking moment

The cross-section stress-strain distribution of elastic stage is shown in figure 16, where x is the vertical distance of any point to the tensile edge of cross-section.

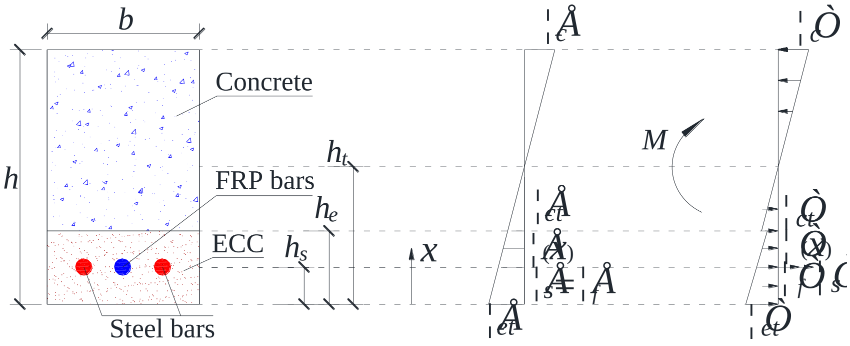

Fig.16 Cross-section stress-strain distribution of elastic stage

The cross-section strain distribution can be expressed as:

$$\varepsilon(x)=\begin{cases}(1-x/h_{\mathrm{t}})\,\varepsilon_{\mathrm{et}} & ,0\le x\le h_{\mathrm{t}}\\(x/h_{\mathrm{t}}-1)\,\varepsilon_{\mathrm{et}} & ,h_{\mathrm{t}}<x\le h\end{cases} \tag{23}$$

According to the force equilibrium of cross-section, $\sum N$ =0, the following equation can be obtained,

$$\int_0^{h_{\mathrm{e}}}\sigma_{\mathrm{et}}(x)b\,dx+\int_{h_{\mathrm{e}}}^{h_{\mathrm{t}}}\sigma_{\mathrm{ct}}(x)b\,dx+E_{\mathrm{s}}\varepsilon_{\mathrm{s}}A_{\mathrm{s}}+E_{\mathrm{f}}\varepsilon_{\mathrm{f}}A_{\mathrm{f}}=\int_{h_{\mathrm{t}}}^{h}\sigma_{\mathrm{c}}(x)b\,dx \tag{24}$$

If ECC cracks before concrete, the maximum ECC tensile strain $\varepsilon_{\mathrm{et}} = \varepsilon_{\mathrm{etc}}$. Similarly, h_{t}, $\varepsilon_{\mathrm{ct}}$, ε_{s} and ε_{f} can be expressed by variable ε_{c}, $h_{\mathrm{t}} = \varepsilon_{\mathrm{etc}}\, h / (\varepsilon_{\mathrm{c}} + \varepsilon_{\mathrm{etc}})$, $\varepsilon_{\mathrm{s}} = \varepsilon_{\mathrm{f}} = \varepsilon_{\mathrm{etc}} - (\varepsilon_{\mathrm{c}} + \varepsilon_{\mathrm{etc}})\, h_{\mathrm{s}} / h$, $\varepsilon_{\mathrm{ct}} = \varepsilon_{\mathrm{etc}} - (\varepsilon_{\mathrm{c}} + \varepsilon_{\mathrm{etc}})\, h_{\mathrm{e}} / h$.

On the other hand, if concrete cracks before ECC, the maximum tensile strain in concrete $\varepsilon_{\mathrm{ct}} = \varepsilon_{\mathrm{ctu}}$. Assuming ε_{c} as a basic variable, h_{t}, $\varepsilon_{\mathrm{et}}$, ε_{s} and ε_{f} can be expressed by variable ε_{c}, $h_{\mathrm{t}} = (h\, \varepsilon_{\mathrm{ctu}} + h_{\mathrm{e}}\, \varepsilon_{\mathrm{c}}) / (\varepsilon_{\mathrm{c}} + \varepsilon_{\mathrm{ctu}})$, $\varepsilon_{\mathrm{s}} = \varepsilon_{\mathrm{f}} = ((h - h_{\mathrm{s}})\, \varepsilon_{\mathrm{ctu}} + (h_{\mathrm{e}} - h_{\mathrm{s}})\, \varepsilon_{\mathrm{c}}) / (h - h_{\mathrm{e}})$, $\varepsilon_{\mathrm{et}} = h\, (\varepsilon_{\mathrm{ctu}} + \varepsilon_{\mathrm{c}}) / (h - h_{\mathrm{e}}) - \varepsilon_{\mathrm{c}}$.

Substituting ε_{c}, h_{t}, $\varepsilon_{\mathrm{et}}$, $\varepsilon_{\mathrm{ct}}$, ε_{s} and ε_{f} into formula (21), then concrete compressive strain ε_{c} can be calculated. And then, according to the moment equilibrium of cross-section, $\sum M$ = 0, cracking moment formula can be expressed as below:

$$M_{\mathrm{cr}} = \int_{h_{\mathrm{t}}}^{h} \sigma_{\mathrm{c}}\left(x\right) bxdx - \int_{0}^{h_{\mathrm{e}}} \sigma_{\mathrm{et}}\left(x\right) bxdx - \int_{h_{\mathrm{e}}}^{h_{\mathrm{t}}} \sigma_{\mathrm{ct}}\left(x\right) bxdx - \left(E_{\mathrm{s}}\varepsilon_{\mathrm{s}}A_{\mathrm{s}} + E_{\mathrm{f}}\varepsilon_{\mathrm{f}}A_{\mathrm{f}}\right) h_{\mathrm{s}} \tag{25}$$

Comparisons of cracking modes and cracking moments are shown in table 5.

Table 5 Comparison of experimental and predicted cracking moments

Beam notation	$M_{\mathrm{cr,e}}$ (kN·m)	$M_{\mathrm{cr,c}}$ (kN·m)	$M_{\mathrm{cr,c}}$ / $M_{\mathrm{cr,e}}$	CM-E	CM-D	CM-A
HB1	3.26	3.08	0.95	—	—	—
HB2	3.74	3.70	0.94	C	C	C
HB3	3.75	3.67	0.94	E	E	E
HB5	3.26	3.20	0.98	—	—	—
HC1	3.26	3.15	0.97	—	—	—
HC2	4.00	3.75	0.94	C	C	C
HC3	3.74	3.72	1.00	E	E	E
HC5	3.56	3.35	0.94	—	—	—
HD1	3.00	2.89	0.96	—	—	—
HD2	3.26	3.20	0.98	E	C	C
HD3	3.25	3.13	0.96	E	E	E
HD5	3.00	2.79	0.93	—	—	—
HE1	3.02	2.96	0.98	—	—	—
HE2	3.39	3.33	0.99	C	C	C
HE3	3.71	3.28	0.88	E	E	E
HE5	3.23	2.93	0.91	—	—	—
HF1	3.26	3.02	0.93	—	—	—
HF2	3.75	3.48	0.93	C	C	C
HF3	3.77	3.43	0.91	E	E	E
HF5	3.33	3.06	0.92	—	—	—
HG1	3.46	3.15	0.91	—	—	—
HG2	3.82	3.75	0.98	C	C	C
HG3	3.80	3.72	0.98	E	E	E
HG5	3.55	3.35	0.94	—	—	—
HH1	3.49	3.15	0.90	—	—	—
HH2	3.75	3.75	1.00	C	C	C
HH3	3.99	3.72	0.93	E	E	E
HH5	3.59	3.35	0.93	—	—	—
HK1	3.02	2.77	0.92	—	—	—
HK2	3.97	3.75	0.93	E	C	C
HK3	3.66	3.72	0.93	E	E	E
HK5	3.73	3.51	0.94	—	—	—
Average values			0.95			
Variation coefficient			0.03			

Note: $M_{cr,e}$ is experimental cracking moment, $M_{cr,c}$ is calculated cracking moment, CM-E is experimental cracking mode, CM-D is cracking mode based on the discriminate formula, CM-A is cracking mode based on cross-section analysis, E means ECC cracking first and C means concrete cracking first, specimen HD2 has initial crack on layer of ECC.

As can be seen from table 5, average values and variation coefficient of $M_{cr,c}$ / $M_{cr,e}$ are 0.95 and 0.03, respectively, indicating good agreement between the predicted and experimental results. The predictions of the first crack location, i.e. in ECC or concrete first, from discriminate formula and cross-section analysis are in good agreement with that observed in experiments, except for specimen HD2 that initially cracked in ECC.

Yield moment

The cross-section stress-strain distribution for this case is shown in figure 17.

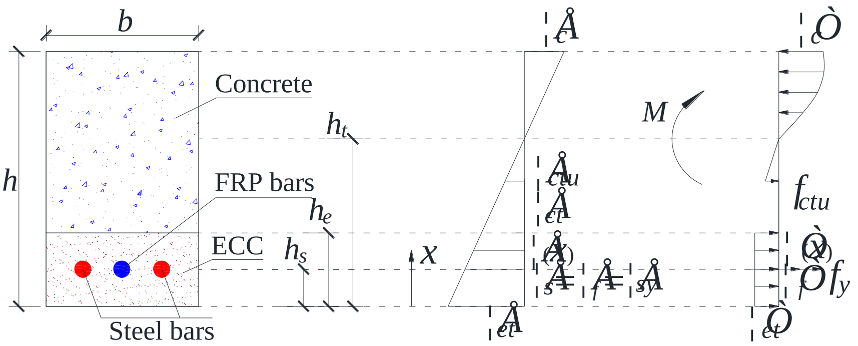

Fig.17 Cross-section stress-strain distribution of composites beams when steel yielded

In this situation, the tensile strain in steel bars $\varepsilon_s = \varepsilon_f = \varepsilon_{sy}$. Assuming ε_c as a basic variable, h_t, ε_{ct} and ε_{et} can be expressed in terms of ε_c, $h_t = \varepsilon_{sy}\,(h - h_s) / (\varepsilon_c + \varepsilon_{sy}) + h_s$, $\varepsilon_{et} = \varepsilon_{sy} + (\varepsilon_c + \varepsilon_{sy})\, h_s / (h - h_s)$, $\varepsilon_{ct} = \varepsilon_{sy} - (\varepsilon_c + \varepsilon_{sy})\,(h_e - h_s) / (h - h_s)$.

According to the force equilibrium of cross-section, $\sum N = 0$, the following equation can be obtained,

$$\int_0^{h_\mathrm{e}}\sigma_\mathrm{et}(x)bdx+\int_{h_\mathrm{e}}^{h_\mathrm{t}}\sigma_\mathrm{ct}(x)bdx+f_\mathrm{y}A_\mathrm{s}+E_\mathrm{f}\varepsilon_\mathrm{f}A_\mathrm{f}=\int_{h_\mathrm{t}}^{h}\sigma_\mathrm{c}(x)bdx \tag{26}$$

Substituting ε_c, h_t, ε_et, ε_sy and ε_ct into formula (23), then concrete compressive strain ε_c can be calculated. According to the moment equilibrium of cross-section, $\sum M = 0$, the yield moment can, then, be expressed as below:

$$M_\mathrm{y}=\int_{h_\mathrm{t}}^{h}\sigma_\mathrm{c}(x)bxdx-\int_0^{h_\mathrm{e}}\sigma_\mathrm{et}(x)bxdx-\int_{h_\mathrm{e}}^{h_\mathrm{t}}\sigma_\mathrm{ct}(x)bxdx-\left(f_\mathrm{y}A_\mathrm{s}+E_\mathrm{f}\varepsilon_\mathrm{sy}A_\mathrm{f}\right)h_\mathrm{s} \tag{27}$$

Comparisons of experimental and predicted yield moments are shown in table 6.

Table 6 Comparison of experimental and predicted yield moments

Beam notation	$M_{y,e}$ (kN·m)	$M_{y,c}$ (kN·m)	$M_{y,c}$ / $M_{y,e}$	Beam notation	$M_{y,e}$ (kN·m)	$M_{y,c}$ (kN·m)	$M_{y,c}$ / $M_{y,e}$
HB1	14.7	13.3	0.90	HF1	8.71	10.8	1.24
HB2	16.2	15.5	0.96	HF2	11.2	13.0	1.16
HB3	17.9	16.8	0.94	HF3	12.4	14.4	1.16
HB5	17.4	15.7	0.90	HF5	12.4	15.0	1.21
HC1	14.0	12.9	0.92	HG1	17.3	14.8	0.86
HC2	17.4	15.2	0.87	HG2	17.5	16.9	0.97
HC3	19.6	16.5	0.84	HG3	18.8	18.9	1.01
HC5	16.9	16.2	0.96	HG5	18.4	18.7	1.02
HD1	7.02	6.83	0.97	HH1	19.5	18.9	0.97
HD2	9.45	9.14	0.97	HH2	23.2	21.1	0.91
HD3	10.7	10.6	0.99	HH3	23.9	22.4	0.94
HD5	10.7	11.3	1.06	HH5	23.7	22.5	0.95
HE1	9.28	8.94	0.96	HK1	—	—	—
HE2	14.0	11.2	0.80	HK2	—	—	—
HE3	13.4	12.6	0.94	HK3	—	—	—
HE5	13.7	13.3	0.97	HK5	—	—	—

Note: $M_{y,e}$ is the experimental yield moment whereas $M_{y,c}$ is the calculated yield moment.

As can be seen from table 5, average values and variation coefficient of $M_{y,c}$ / $M_{y,e}$ are 0.98 and 0.10, respectively, indicating good agreement between the predicted and experimental yield moments.

Ultimate moment

The cross-section stress-strain distribution when concrete is crushed is shown in figure 18.

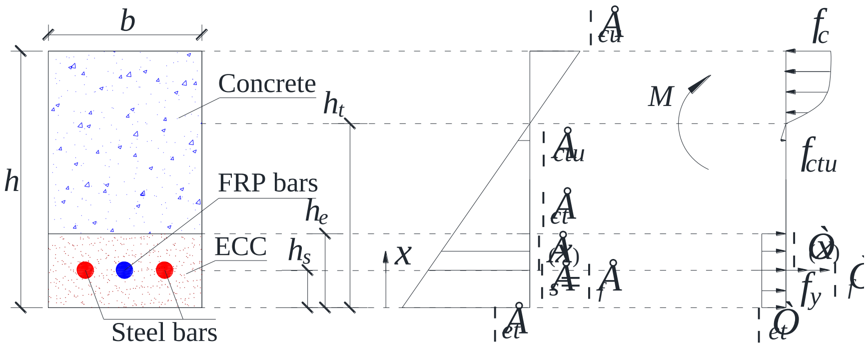

Fig.18 Cross-section stress-strain distribution – when concrete crushed after steel yielding

In this situation, the maximum compressive strain in concrete $\varepsilon_c = \varepsilon_{cu}$. Assuming ε_{et} as a basic variable, h_t, ε_{ct}, ε_s and ε_f can be expressed in terms of ε_{et}, $h_t = \varepsilon_{et}\, h / (\varepsilon_{cu} + \varepsilon_{et})$, $\varepsilon_s = \varepsilon_f = \varepsilon_{et} - (\varepsilon_{cu} + \varepsilon_{et})\, h_s / h$, $\varepsilon_{ct} = \varepsilon_{et} - (\varepsilon_{cu} + \varepsilon_{et})\, h_e / h$.

Substituting ε_c, h_t, ε_{et}, ε_s, ε_f and ε_{ct} into formula (23), then, the maximum ECC tensile strain ε_{et} can be calculated. According to the moment equilibrium of cross-section, $\sum M = 0$, ultimate moment can, then, be expressed as below:

$$M_u = \int_{h_t}^{h} \sigma_c(x)bxdx - \int_0^{h_e} \sigma_{et}(x)bxdx - \int_{h_e}^{h_t} \sigma_{ct}(x)bxdx - \left(f_y A_s + E_f \varepsilon_f A_f\right)h_s \tag{28}$$

If the composite beam is over-reinforced, steel bar does not yield while the concrete compressive strain reaches the ultimate compressive strain and the beam incurs brittle failure. In this case, $\varepsilon_s = \varepsilon_f \leq \varepsilon_{sy}$. Assuming ε_{et} as a basic variable, h_t, ε_{ct}, ε_s and ε_f can be expressed by variable ε_{et}, $h_t = \varepsilon_{et}\ h / (\varepsilon_{cu} + \varepsilon_{et})$, $\varepsilon_s = \varepsilon_f = \varepsilon_{et} - (\varepsilon_{cu} + \varepsilon_{et})\, h_s / h$, $\varepsilon_{ct} = \varepsilon_{et} - (\varepsilon_{cu} + \varepsilon_{et})\, h_e / h$. Substituting ε_c, h_t, ε_{et}, ε_s, ε_f and ε_{ct} into formula (21), then the maximum ECC tensile strain ε_{et} can be calculated. According to the equilibrium of cross-section moment $\sum M = 0$, the ultimate moment can, then, be expressed as below:

$$M_u = \int_{h_t}^{h} \sigma_c(x)bxdx - \int_0^{h_e} \sigma_{et}(x)bxdx - \int_{h_e}^{h_t} \sigma_{ct}(x)bxdx - (E_s \varepsilon_s A_s + E_f \varepsilon_f A_f)h_s \tag{29}$$

If steel bars reach their ultimate tensile strain first, the tensile strain in bars $\varepsilon_s = \varepsilon_f = \varepsilon_{su}$, $h_t = \varepsilon_{su}\,(h - h_s) / (\varepsilon_c + \varepsilon_{su}) + h_s$, $\varepsilon_{et} = \varepsilon_{su} + (\varepsilon_c + \varepsilon_{su})\, h_s / (h - h_s)$, $\varepsilon_{ct} = \varepsilon_{su} - (\varepsilon_c + \varepsilon_{su})\,(h_e - h_s) / (h - h_s)$. Substituting

ε_c, h_t, ε_{et}, ε_s, ε_f and ε_{ct} into formula (23), then concrete compressive strain ε_c can be calculated. According to the equilibrium of cross-section moment $\sum M = 0$, the ultimate moment can, then, be expressed as below:

$$M_u = \int_{h_t}^{h} \sigma_c(x)bxdx - \int_{0}^{h_e} \sigma_{et}(x)bxdx - \int_{h_e}^{h_t} \sigma_{ct}(x)bxdx - (f_y A_s + E_f \varepsilon_{su} A_f)h_s \tag{30}$$

If FRP bars rupture first, the tensile strain in bars $\varepsilon_s = \varepsilon_f = \varepsilon_{fu}$, $h_t = \varepsilon_{fu}(h - h_s) / (\varepsilon_c + \varepsilon_{fu}) + h_s$, $\varepsilon_{et} = \varepsilon_{fu} + (\varepsilon_c + \varepsilon_{fu})\, h_s / (h - h_s)$, $\varepsilon_{ct} = \varepsilon_{fu} - (\varepsilon_c + \varepsilon_{fu})\,(h_e - h_s) / (h - h_s)$. Substituting ε_c, h_t, ε_{et}, ε_s, ε_f and ε_{ct} into formula (23), then concrete compressive strain ε_c can be calculated. According to the equilibrium of cross-section moment $\sum M = 0$, the ultimate moment can, then, be expressed as below:

$$M_u = \int_{h_t}^{h} \sigma_c(x)bxdx - \int_{0}^{h_e} \sigma_{et}(x)bxdx - \int_{h_e}^{h_t} \sigma_{ct}(x)bxdx - (f_y A_s + f_u A_f)h_s \tag{31}$$

Loading-deflection curves

After the whole process of cross-section analysis of composite beams is completed, the load-deflection curves of specimens can be obtained (Xu et al. 2009). The comparisons of experimental and calculated load-deflection curves of group HG are shown in figure 19.

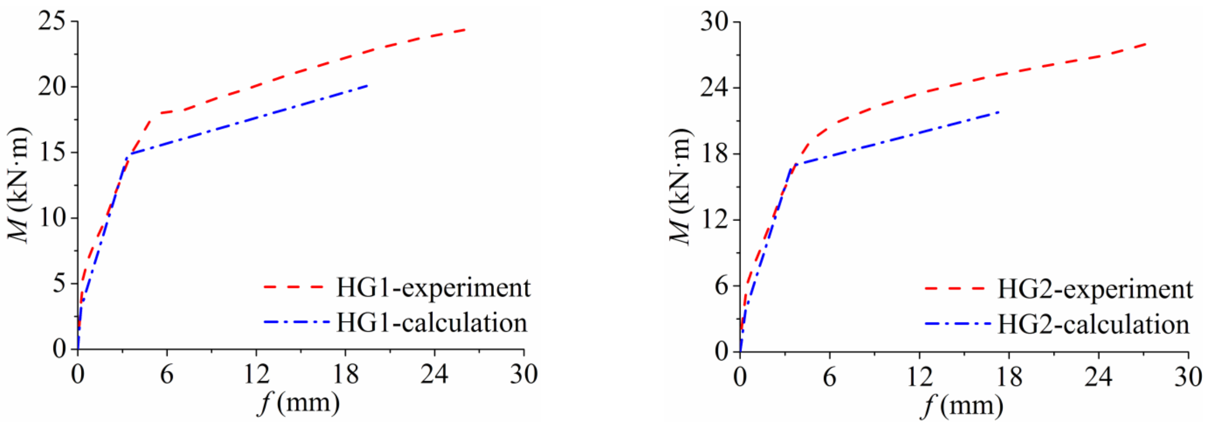

(a) HG1 (b) HG2

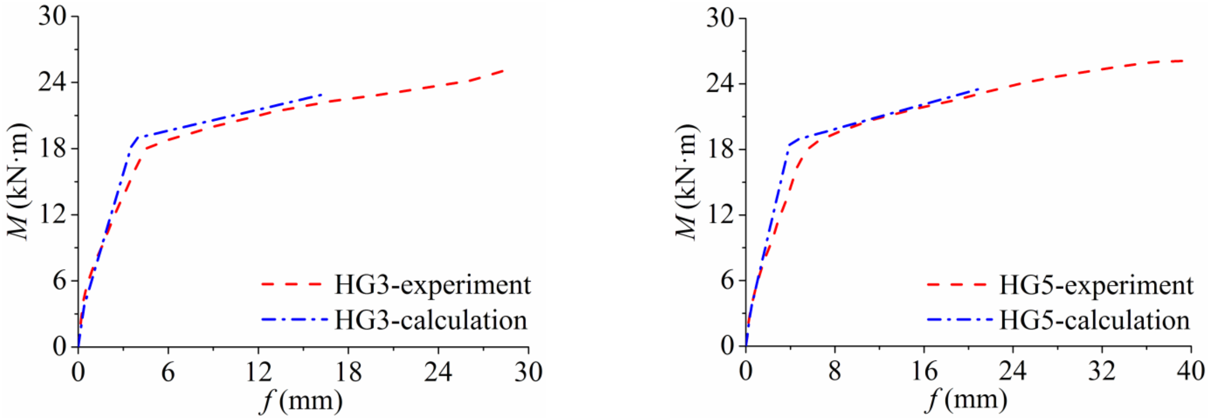

(c) HG3 (d) HG5

Fig.19 Comparisons of experimental and calculated moment-deflection curves

As can be seem from the figure 19, experimental and calculated curves fit well.

Parametric study

In this section of the paper, the effect of various parameters including the strength, height replacement ratio and ultimate tensile strain of ECC, strength, elastic modulus and amount of reinforcement, compressive strength and ultimate compressive strain of concrete on the flexural behavior (cracking moment M_{cr}, yield moment M_y, ultimate moment M_u, yield curvature φ_y, ultimate curvature φ_u, ductility u_φ and energy dissipation E_φ) of FRP reinforced ECC-concrete composite beams is considered.

When one parameter is changed, other basic parameters are kept constant at the following values: ECC height replacement ratio r_h is 0.29, reinforcement ratio are ρ_A ($\rho_{s,A} + \rho_{f,A}$ = 0.6% + 0.3%) and ρ_B ($\rho_{s,B} + \rho_{f,B}$ = 0.3% + 0.6%), respectively, yield strength of steel reinforcement f_{yk} is 400 MPa, compressive strength of concrete f_c is 28.6 MPa and its ultimate compressive strain ε_{cu} is 0.0033, ECC tensile strength at first cracking f_{etc} is 5.0 MPa and its corresponding strain ε_{etc} is 0.0003, ECC ultimate tensile strength f_{etu} is 1.2 times of f_{etc} and its corresponding strain ε_{etu} is 0.03.

The composite beam cross-section is assumed to be failed when maximum concrete compressive strain, ε_c, tensile strains in reinforcement, ε_s, or tensile strains in ECC, ε_{et}, reaches their ultimate strain, respectively. The failure modes can be predicted by the proposed model, namely failure mode ① (over-reinforced failure - concrete compressive strain reaches ε_{cu} before yielding of steel reinforcement), failure mode ② (compressive failure - concrete compressive strain reaches ε_{cu} after yielding of steel reinforcement), failure mode ③ (tensile failure 1 - tensile strain in reinforcement reaches ε_{hu} first) and failure mode ④ (tensile failure 2 - tensile strain in ECC reaches ε_{etu} first). All specimens occur compressive failure (failure mode ②) according to formulas (21) ~ (22).

Ⅰ Strength, height replacement ratio and ultimate tensile strain of ECC

The effect of ECC strength, ECC height replacement ratio and ECC ultimate tensile strain on the flexural behavior are shown in figures 20 ~ 22. Seven ECC tensile strengths f_{etc} (2.0 MPa, 3.0 MPa, 4.0 MPa, 5.0 MPa, 6.0 MPa, 7.0 MPa and 8.0 MPa), five ECC height replacement ratios r_h (0, 0.14, 0.29, 0.43 and 0.57) and five ECC ultimate tensile strains ε_{etu} (0.02, 0.03, 0.04, 0.05 and 0.06) are studied.

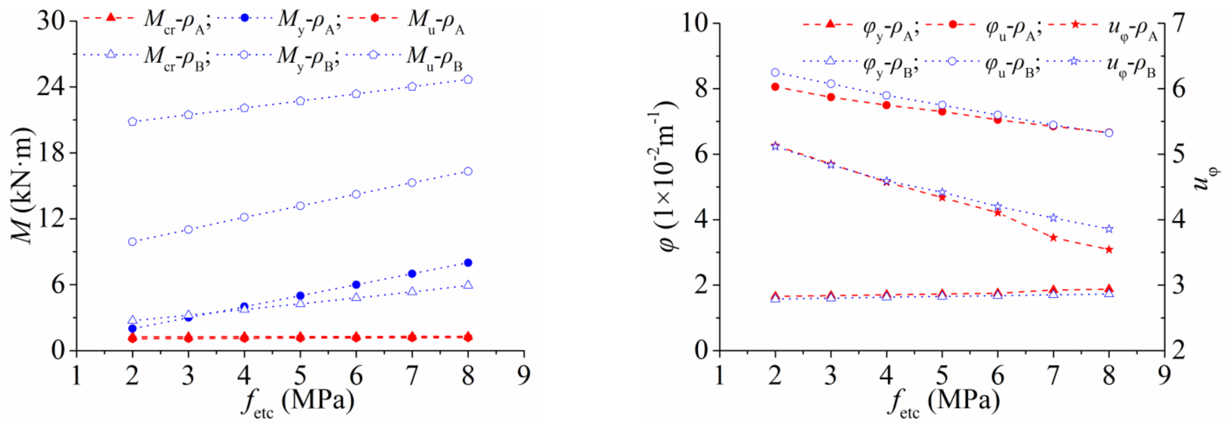

(a) Cracking, yield and ultimate moment (b) Yield curvature, ultimate curvature and ductility

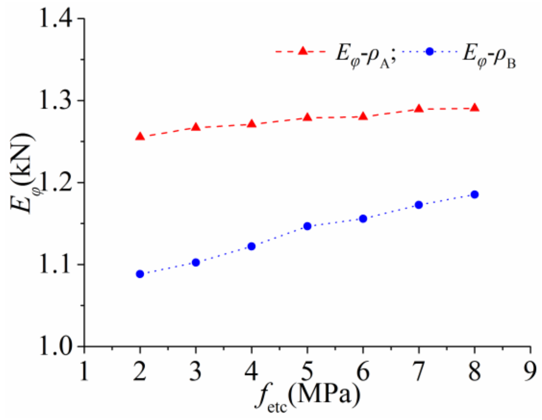

(c) Energy dissipation

Fig.20 Effect of ECC strength

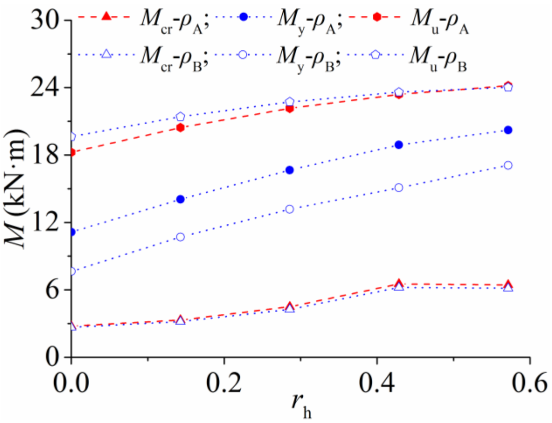

(a) Cracking, yield and ultimate moment

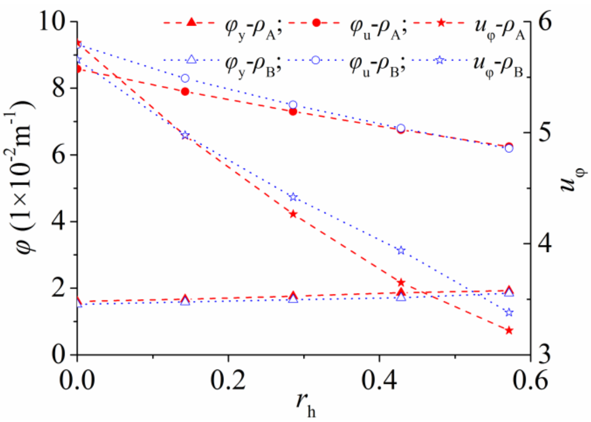

(b) Yield curvature, ultimate curvature and ductility

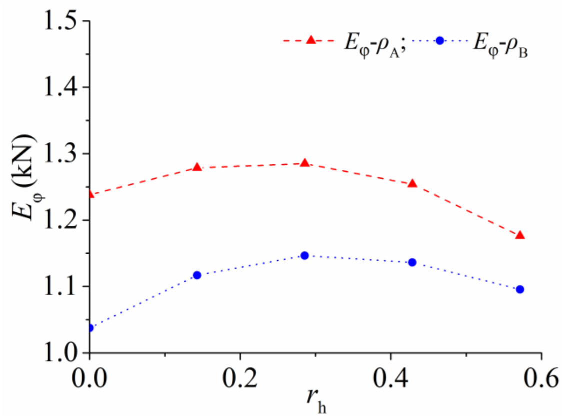

(c) Energy dissipation

Fig.21 Effect of ECC height replacement ratio

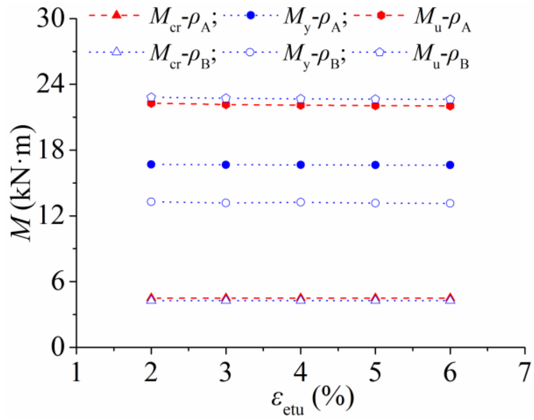

(a) Cracking, yield and ultimate moment

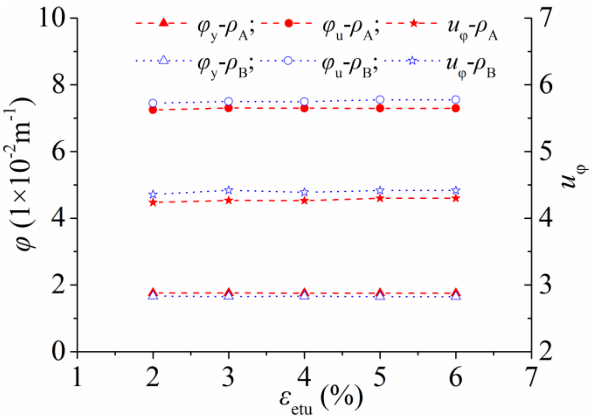

(b) Yield curvature, ultimate curvature and ductility

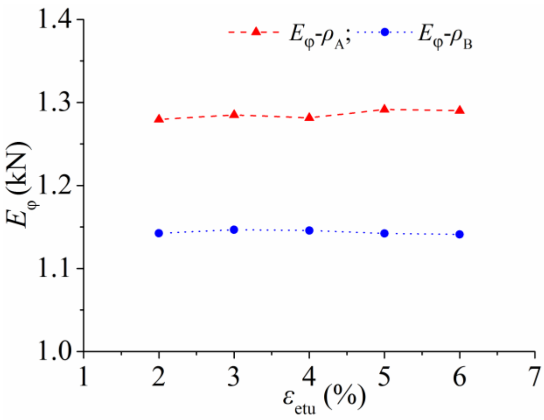

(c) Energy dissipation

Fig.22 Effect of ECC ultimate tensile strain

As can be seen from figures 20 and 21, the cracking, yield and ultimate moments increase with increasing the strength or the height replacement ratio of ECC. The yield curvature gradually increases while the ultimate curvature gradually decreases with increasing the strength or the height replacement ratio of ECC. So, the curvature ductility decreases with increasing the strength or the height replacement ratio of ECC. With increasing the strength of ECC, the energy dissipation gradually increases. With increasing the height replacement ratio of ECC, the energy dissipation, initially, increases and, then, decreases.

For all specimens compressive failure occurs (failure mode ②) - crushing of concrete after yielding of steel reinforcement and, therefore, ECC ultimate tensile strain has no significant influence on the flexural behavior of composite beams as indicated in figure 22.

Ⅱ Strength, elastic modulus and amount of reinforcement

The effect of yield strength of steel reinforcement, ultimate tensile strength and elastic modulus of FRP reinforcement, amount of reinforcement on the flexural behavior is shown in figures 23 ~ 26. Four yield strengths of steel reinforcement f_{yk} (300 MPa, 400 MPa, 500 MPa and 600 MPa), four elastic moduli of FRP reinforcement E_f (50 GPa, 75 GPa, 100 GPa and 125 GPa), five ultimate tensile strengths of FRP reinforcement f_{fu} (600 MPa, 900 MPa, 1200 MPa, 1500 MPa and 1800 MPa) and three groups of reinforcement (group 1: ρ_h = 0.6 %, $\rho_{h,E}$ = 0.15 %, 0.3 % and 0.60 %, respectively; group 2: ρ_h = 0.9 %, $\rho_{h,E}$ = 0.22 %, 0.45 %, 0.67 % and 0.90 %, respectively; group 3: ρ_h = 1.2 %, $\rho_{h,E}$ = 0.52 %, 0.75 % and 0.97 %, respectively) are studied.

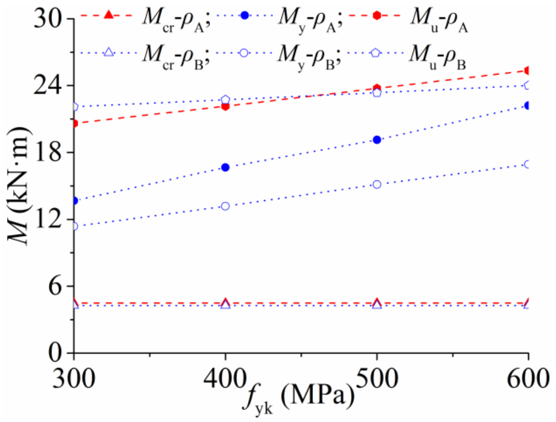

(a) Cracking, yield and ultimate moment

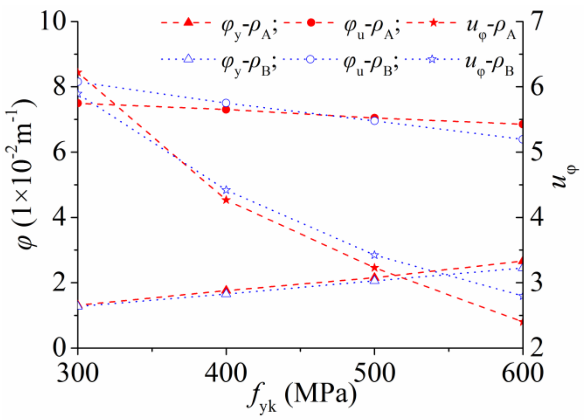

(b) Yield curvature, ultimate curvature and ductility

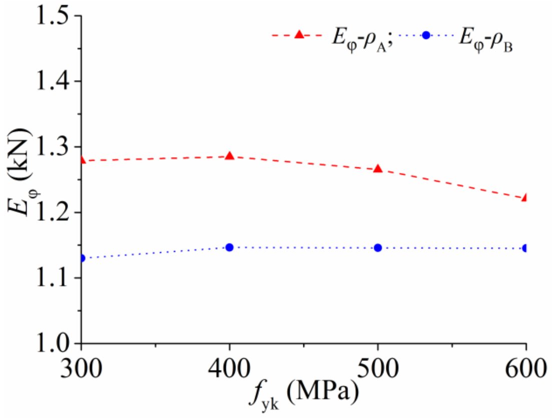

(c) Energy dissipation

Fig.23 Effect of steel yield strength

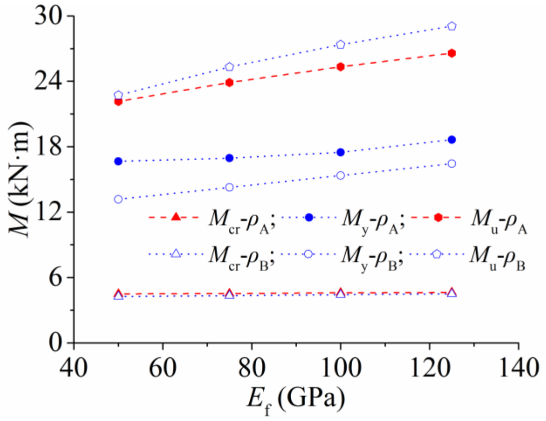

(a) Cracking, yield and ultimate moment

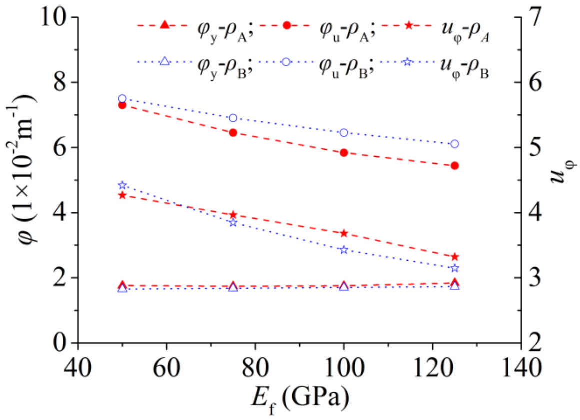

(b) Yield curvature, ultimate curvature and ductility

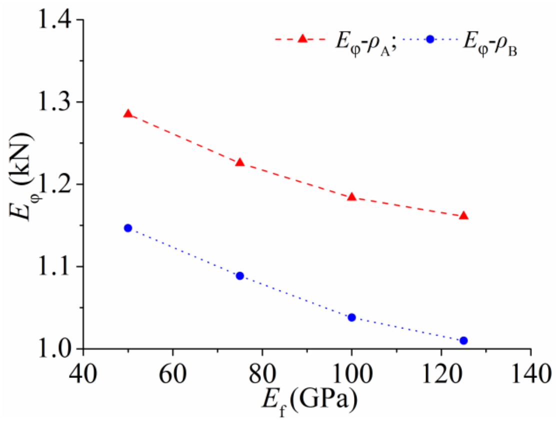

(c) Energy dissipation

Fig.24 Effect of FRP elastic modulus

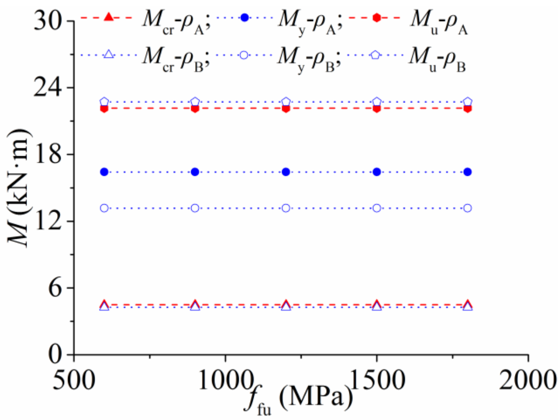

(a) Cracking, yield and ultimate moment

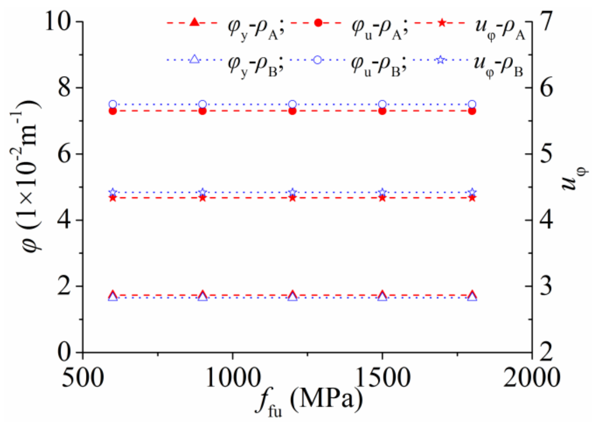

(b) Yield curvature, ultimate curvature and ductility

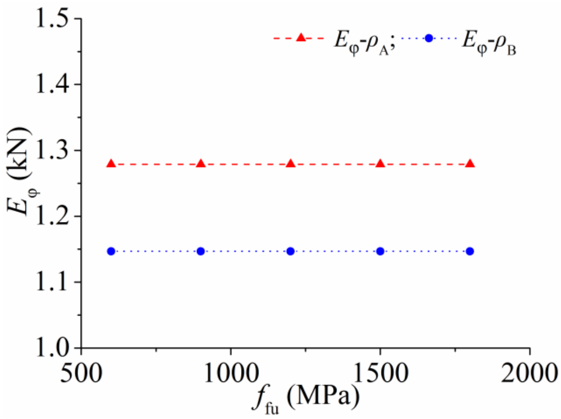

(c) Energy dissipation

Fig.25 Effect of FRP ultimate tensile strength

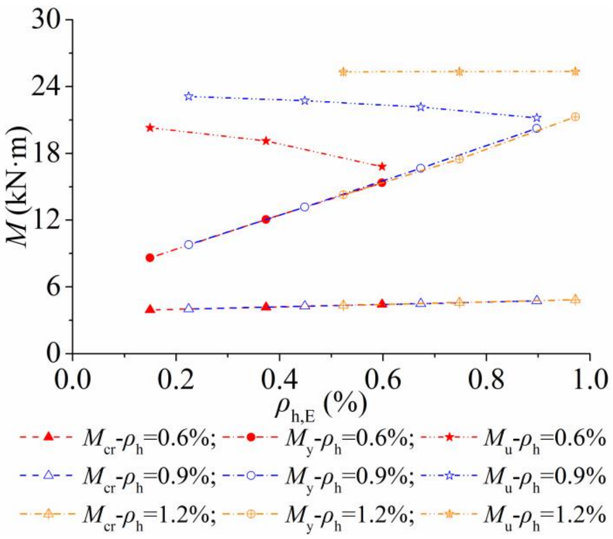

(a) Cracking, yield and ultimate moment

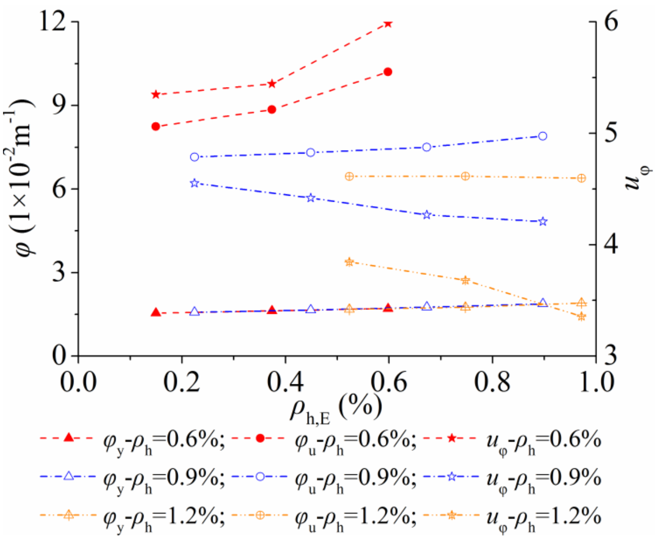

(b) Yield curvature, ultimate curvature and ductility

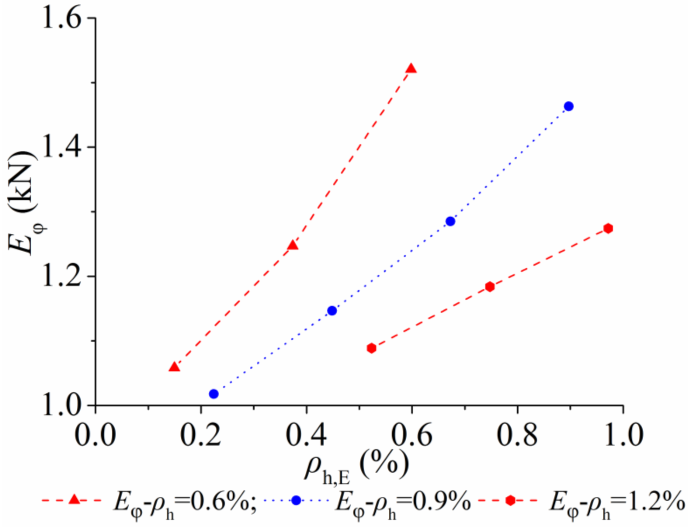

(c) Energy dissipation

Fig.26 Effect of the nominal reinforcement ratio using elastic modulus conversion ratio

As can be seen from figures 23 ~ 26, the yield and ultimate moments increase with increasing the yield strength of steel reinforcement or the elastic modulus of FRP reinforcement. The cracking moments slightly increase with increasing the elastic modulus of FRP reinforcement while the yield strength of steel reinforcement has no effect on the cracking moment.

With increasing the yield strength of steel reinforcement or the elastic modulus of FRP reinforcement, the yield curvature gradually increases while the ultimate curvature gradually decreases, and the curvature ductility decreases accordingly. With increasing the yield strength of steel reinforcement, the energy dissipation, initially, increases and, then, decreases. With increasing the elastic modulus of FRP reinforcement, the energy dissipation gradually decreases.

For all specimens compressive failure occurs (failure mode ②) - crushing of concrete after yielding of steel reinforcement and, therefore, the ultimate tensile strength of FRP reinforcement has no effect on the flexural behavior of composite beams as presented in figure 25.

With increasing the nominal reinforcement ratio using elastic modulus conversion ratio, cracking moment slightly increases, the yield moment significantly increases and the ultimate moment gradually decreases. The ultimate moment decreasing rate decreases with the increase of the practical reinforcement ratio. The yield curvature and ultimate curvature gradually increase, and the ultimate curvature increasing rate decreases with increasing the practical reinforcement ratio. The curvature ductility of specimens with lower practical reinforcement ratio (group 1) increases while curvature ductility of specimens with higher practical reinforcement ratio (group 2 and 3) decreases with increasing the nominal reinforcement ratio using elastic modulus conversion ratio. The energy dissipation gradually increases with increasing the nominal reinforcement ratio using elastic modulus conversion ratio.

Ⅲ Compressive strength and ultimate compressive strain of concrete

The effect of concrete compressive strength and ultimate compressive strain on the flexural behavior is shown in figures 27 ~ 28. Eight concrete strengths f_c (16.7 MPa, 20.1 MPa, 23.4 MPa, 26.8 MPa, 29.6 MPa, 32.4 MPa, 35.5 MPa and 38.5 MPa) and four concrete ultimate compressive strains f_{fu} (0.003, 0.0035, 0.004 and 0.005) are studied.

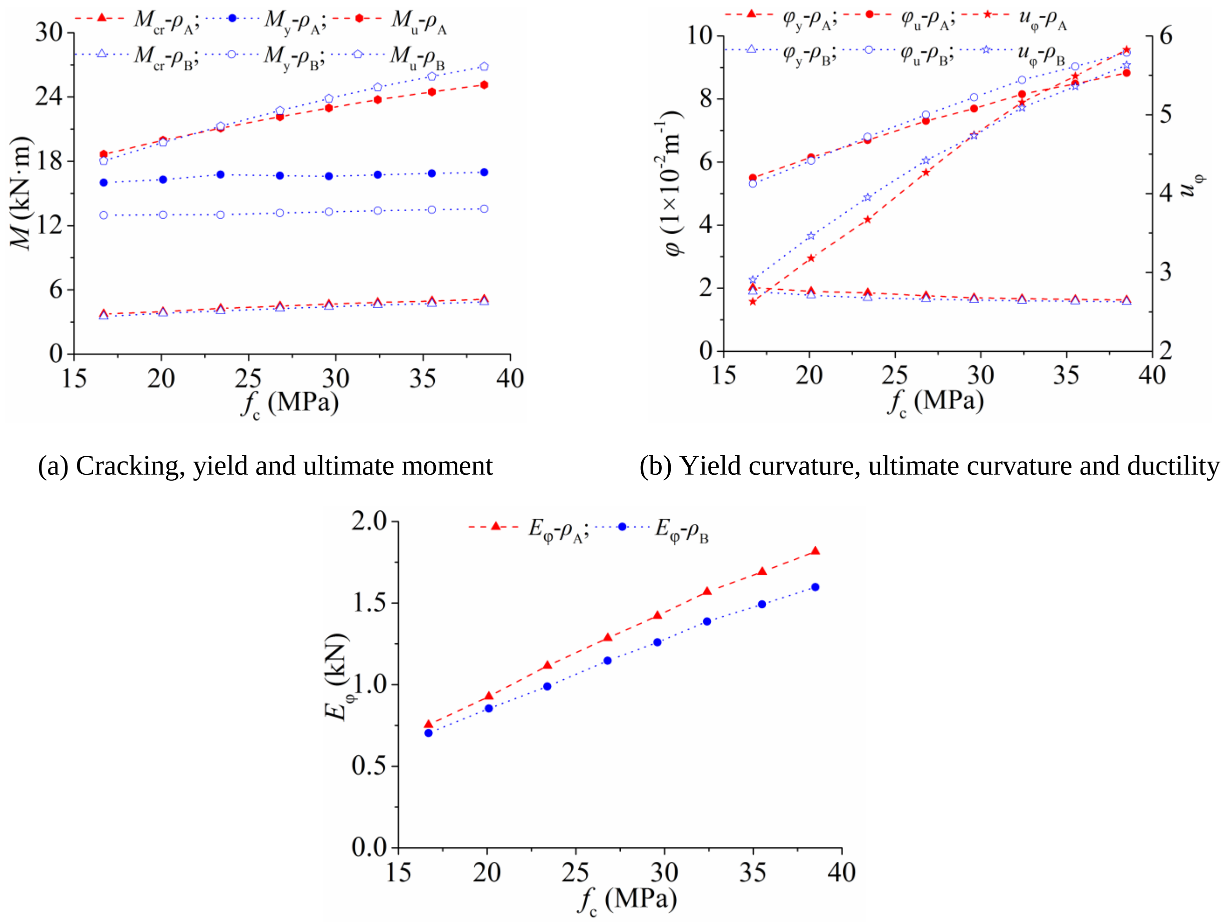

(a) Cracking, yield and ultimate moment

(b) Yield curvature, ultimate curvature and ductility

(c) Energy dissipation

Fig.27 Effect of concrete compressive strength

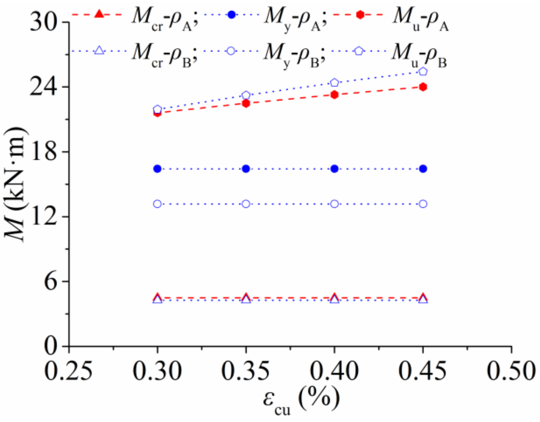

(a) Cracking, yield and ultimate moment

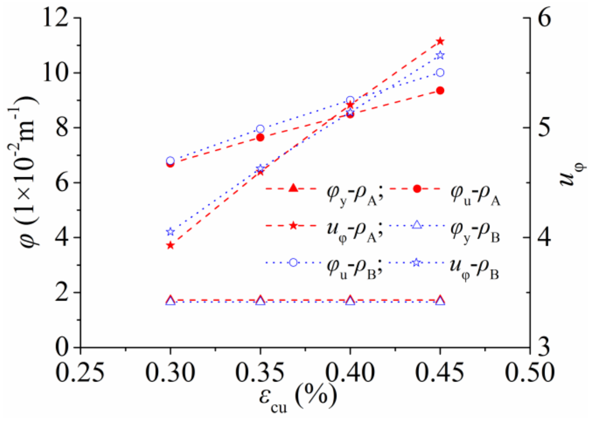

(b) Yield curvature, ultimate curvature and ductility

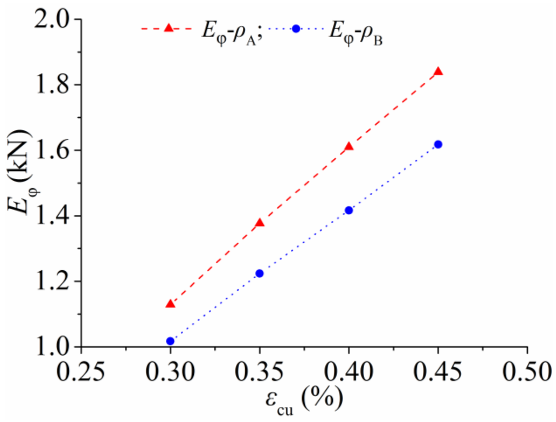

(c) Energy dissipation

Fig.28 Effect of concrete ultimate compressive strain

As can be seen from figures 27 and 28, the cracking, yield and ultimate moments increase with the increase of the strength of concrete. With increasing the concrete ultimate compressive strain, the ultimate moments gradually increase while the cracking and yield moments keep constant.

The yield curvature slightly decreases with increasing the concrete compressive strength while concrete ultimate compressive strain has no effect on the yield curvature. The ultimate curvature significantly increases with increasing the concrete compressive strength. So, the curvature ductility and the energy dissipation significantly increase with increasing the concrete compressive strength.

Simplified calculation of ultimate moment

In this section, a simplified calculation of section ultimate moment is developed. It is mainly based on a simplified rectangular stress block of concrete stresses in compression and ECC in tension. Two cases are proposed as explained below.

Hybrid reinforced ECC-concrete composite beams

The simplified cross-section stress-strain distribution when the appropriate hybrid reinforced composite beam incurs failure is shown in figure 29. The following formula can be obtained according to the force equilibrium of cross-section, where x_c and x are the actual and height of compressive concrete, respectively, $x = \beta_c x_c$, α_c and β_c are coefficients related to the properties of concrete (Chinese National Standard 2010), $\alpha_c = 1.0$ and $\beta_c = 0.8$.

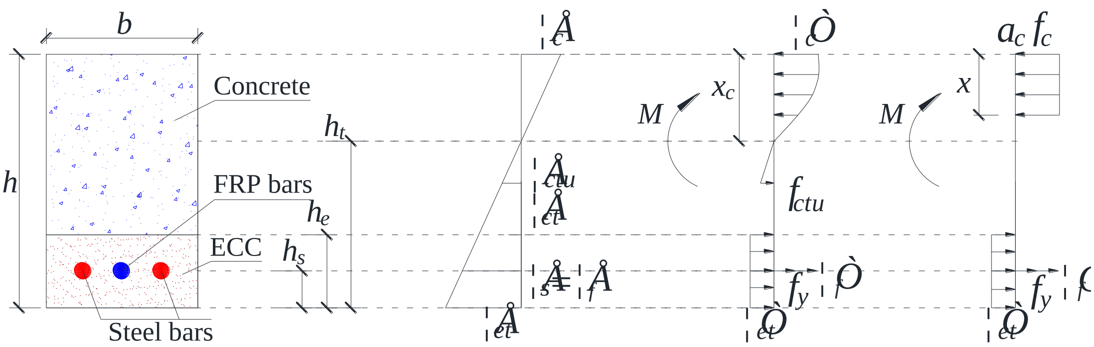

Fig.29 Simplified stress distribution of hybrid reinforced composite beam at failure

$$\alpha_c f_c bx = f_y A_s + E_f \varepsilon_{hu} A_f + f_{etc} bh_e \tag{32}$$

$$\varepsilon_{hu} = \varepsilon_{cu}(\beta_c / \xi - 1) \tag{33}$$

Combining equations (32) and (33), the flexural capacity of hybrid reinforced concrete beams can be calculated by the following simplified formula:

$$\begin{aligned} M_u &= (f_y A_s + E_f \varepsilon_{hu} A_f)(1 - \xi_h / 2)h_0 + f_{etc} bh_e (h - h_e / 2 - \xi_h h_0 / 2) \\ &= \alpha_c f_c bh_0^2 \xi_h (1 - \xi_h / 2) - f_{etc} bh_e (h_e / 2 - h_s / 2) \end{aligned} \tag{34}$$

$$\xi_h = \frac{-B_h + \sqrt{B_h^2 - 4A_h C_h}}{2A_h} \tag{35}$$

where, $A_h = \alpha_c f_c$, $B_h = E_f \varepsilon_{cu} \rho_f - f_y \rho_s - f_{etc} r_h$, $C_h = -E_f \rho_f \varepsilon_{cu} \beta_c$.

As the tension of concrete is neglected when calculating the ultimate moment of concrete beams

(Chinese National Standard 2010), so the formula of ultimate moment of hybrid reinforced composite beams can be also applied to hybrid reinforced concrete beams by just substituting $f_{ect} = 0$.

Hybrid reinforced ECC beams

When areinforced hybrid reinforced ECC beam incurs failure, the actual stress distribution and simplified stress distribution of hybrid reinforced ECC beams are shown in figure 30. The following formulas can be obtained according to force equilibrium of cross-section, where x_e and x are the actual and calculate height of compressive ECC, respectively, $x = \beta_e x_e$; a_e and β_e are coefficients related to the properties of ECC; F_{ec} is the resultant force of compressive ECC.

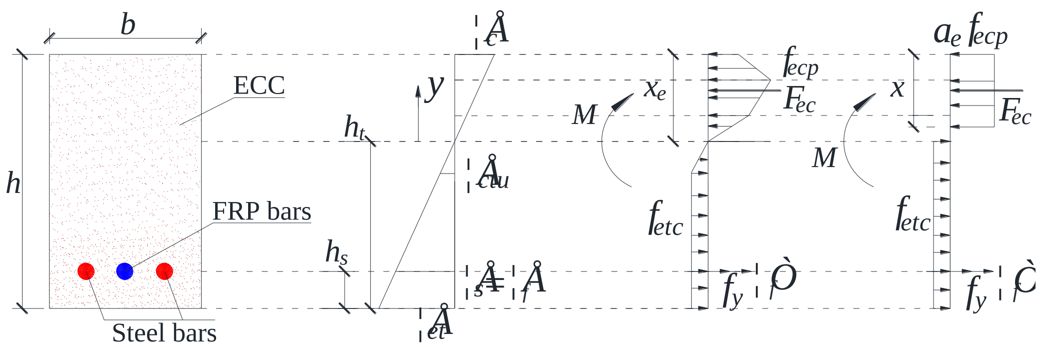

Fig.30 Simplified stress distribution of hybrid reinforced ECC beam at failure

$$\alpha_e f_{ecp} bx = f_y A_s + E_f \varepsilon_{hu} A_f + f_{etc} bh_t \tag{36}$$

$$\varepsilon_{hu} = \varepsilon_{ecu} (\beta_e / \xi - 1) \tag{37}$$

As the resultant stresses and the resultant moment of the compressive force to the neutral axils of actual stress distribution are equal to those of simplified stress distribution, the following formulas can be obtained,

$$\alpha_e f_{ecp} bx = \int_0^{x_e} \sigma_{ec}(y) bdy \tag{38}$$

$$\alpha_e f_{ecp} bx(x_e - x/2) = \int_0^{x_e} \sigma_{ec}(y) bydy \tag{39}$$

Substituting the basic mechanical properties of ECC to equations (38) and (39), α_e and β_e can be obtained, $\alpha_e = 1.0$ and $\beta_e = 0.75$.

And then, according to the moment equilibrium of cross-section, $\sum M = 0$, the flexural capacity of hybrid reinforced ECC beams can be calculated by the following simplified formula:

$$\begin{aligned} M_{\mathrm{u}} &= (f_{\mathrm{y}} A_{\mathrm{s}} + E_{\mathrm{f}} \varepsilon_{\mathrm{hu}} A_{\mathrm{f}})(1 - \xi_{\mathrm{e}}/2) h_0 + f_{\mathrm{etc}} b h_{\mathrm{e}} (h - h_{\mathrm{e}}/2 - \xi_{\mathrm{e}} h_0/2) \\ &= \alpha_{\mathrm{e}} f_{\mathrm{ecp}} b h_0^2 \xi_{\mathrm{e}} (1 - \xi_{\mathrm{e}}/2) - f_{\mathrm{etc}} b h_{\mathrm{e}} (h_{\mathrm{e}}/2 - h_{\mathrm{s}}/2) \end{aligned} \tag{40}$$

$$\xi_{\mathrm{e}} = \frac{-B_{\mathrm{e}} + \sqrt{B_{\mathrm{e}}^2 - 4A_{\mathrm{e}}C_{\mathrm{e}}}}{2A_{\mathrm{e}}} \tag{41}$$

where, $\mathrm{A_e} = \alpha_{\mathrm{e}} f_{\mathrm{ecp}}$, $\mathrm{B_e} = E_{\mathrm{f}}\,\varepsilon_{\mathrm{ecu}}\,\rho_{\mathrm{f}} - f_{\mathrm{etc}}\,r_{\mathrm{h}} - f_{\mathrm{y}}\,\rho_{\mathrm{s}}$, $\mathrm{C_e} = -E_{\mathrm{f}}\,\rho_{\mathrm{f}}\,\varepsilon_{\mathrm{ecu}}\,\beta_{\mathrm{e}}$.

Comparisons of experimental and calculated ultimate moments are shown in table 7.

Table 7 Comparison of ultimate experimental and predicted moments

Beam notation	$M_{u,e}$ (kN·m)	$M_{u,c1}$ (kN·m)	$M_{u,s1}$ (kN·m)	$M_{u,c2}$ (kN·m)	$M_{u,s2}$ (kN·m)	$M_{u,c1}$ / $M_{u,e}$	$M_{u,s1}$ / $M_{u,e}$	$M_{u,c2}$ / $M_{u,e}$	$M_{u,s2}$ / $M_{u,e}$	$M_{u,s1}$ / $M_{u,c1}$	$M_{u,s2}$ / $M_{u,c2}$
HB1	19.3	15.2	15.2	18.5	18.5	0.79	0.79	0.96	0.96	1.00	1.00
HB2	19.5	17.7	17.3	20.9	20.5	0.91	0.89	1.07	1.05	0.98	0.98
HB3	19.8	19.3	18.6	22.3	21.7	0.97	0.94	1.13	1.10	0.96	0.97
HB5	22.5	18.2	20.0	20.7	23.2	0.81	0.89	0.92	1.03	1.10	1.12
HC1	22.0	18.5	18.6	21.5	21.6	0.84	0.85	0.98	0.98	1.01	1.00
HC2	23.9	20.3	20.0	23.3	23.1	0.85	0.84	0.97	0.97	0.99	0.99
HC3	25.7	21.3	20.8	24.3	23.9	0.83	0.81	0.95	0.93	0.98	0.98
HC5	24.8	22.2	21.5	24.9	24.8	0.90	0.87	1.00	1.00	0.97	1.00
HD1	18.3	17.9	17.6	18.5	18.3	0.98	0.96	1.01	1.00	0.98	0.99
HD2	18.6	19.3	19.0	19.9	19.7	1.04	1.02	1.07	1.06	0.98	0.99
HD3	22.0	19.9	19.4	20.5	20.1	0.90	0.88	0.93	0.91	0.97	0.98
HD5	21.9	21.3	19.5	21.9	20.3	0.97	0.89	1.00	0.93	0.92	0.93
HE1	21.2	19.0	19.2	19.9	20.1	0.90	0.91	0.94	0.95	1.01	1.01
HE2	26.8	20.5	20.2	21.4	21.3	0.76	0.75	0.80	0.79	0.99	1.00
HE3	23.6	21.1	20.6	22.1	21.7	0.89	0.87	0.94	0.92	0.98	0.98
HE5	27.1	22.5	20.9	23.4	22.0	0.83	0.77	0.86	0.81	0.93	0.94
HF1	17.3	17.1	17.2	18.6	18.8	0.99	0.99	1.08	1.09	1.01	1.01
HF2	20.1	18.9	18.5	20.4	20.3	0.94	0.92	1.01	1.01	0.98	1.00
HF3	21.4	19.8	19.3	21.4	21.0	0.93	0.90	1.00	0.98	0.97	0.98
HF5	19.7	20.8	20.0	22.3	21.8	1.06	1.02	1.13	1.11	0.96	0.98
HG1	24.3	20.1	20.3	22.4	22.7	0.83	0.84	0.92	0.93	1.01	1.01
HG2	28.3	21.9	21.6	24.2	24.2	0.77	0.76	0.86	0.86	0.99	1.00
HG3	25.1	22.9	22.4	25.2	25.0	0.91	0.89	1.00	1.00	0.98	0.99
HG5	26.8	23.6	23.4	25.7	26.0	0.88	0.87	0.96	0.97	0.99	1.01
HH1	26.6	22.7	22.8	25.9	26.0	0.85	0.86	0.97	0.98	1.00	1.00
HH2	28.8	24.5	24.3	27.7	27.5	0.85	0.84	0.96	0.95	0.99	0.99

HH3	28.7	25.5	25.1	28.7	28.3	0.89	0.87	1.00	0.99	0.98	0.99
HH5	27.2	26.0	26.1	28.7	29.5	0.96	0.96	1.06	1.08	1.00	1.03
HK1	17.8	—	—	18.4	18.5	—	—	1.03	1.04	—	1.01
HK2	20.4	—	—	19.6	19.3	—	—	0.96	0.95	—	0.98
HK3	22.3	—	—	19.9	19.5	—	—	0.89	0.87	—	0.98
HK5	22.0	—	—	19.2	18.0	—	—	0.87	0.82	—	0.94
					u	0.89	0.88	0.98	0.97	0.99	0.99
					CV	0.08	0.08	0.08	0.08	0.03	0.03

Note: $M_{u,e}$ is the experimental ultimate moment; $M_{u,c1}$ and $M_{u,c2}$ are the ultimate moment calculated by derived formula by using of yield strength and ultimate strength of steel bars, respectively; $M_{u,s1}$ and $M_{u,s2}$ are the ultimate moment calculated by simplified formula by using of yield strength and ultimate strength of steel bars, respectively. u and CV are the average value and variation coefficient, respectively.

As can be observed from table 6, the average values of $M_{u,c1} / M_{u,e}$ and $M_{u,s1} / M_{u,e}$ are 0.89 and 0.88, respectively, and their variation coefficients are 0.08 and 0.08, respectively. The ultimate moments calculated by derived and simplified formulas, when yield strength of steel bars used, are lower than the respective experimental ultimate moment for each beam tested. The average values of $M_{u,c2} / M_{u,e}$ and $M_{u,s2} / M_{u,e}$ are 0.98 and 0.97, respectively, and their variation coefficients are 0.08 and 0.08, respectively, indicating good agreement between the predicted and experimental results. The average values of $M_{u,s1} / M_{u,c1}$ and $M_{u,s2} / M_{u,c2}$ are 0.99 and 0.99, respectively, and their variation coefficients are 0.03 and 0.03, indicating good agreement between the calculated ultimate moments of derived formula and simplified formula and experimental results.

Conclusions

Experimental and analytical flexural behavior of hybrid composite beams reinforced with steel and FRP bars are studied. Based on the constitutive models of materials and plane-section assumption, simplified discriminate formulas of cracking mode are developed. Two boundary failure points and three failure modes of hybrid composite beams are proposed, and the discriminate formulas of failure modes are also given. Furthermore, formulas for cracking, yield, ultimate moments are derived. Simplified flexural capacity formulas of hybrid reinforced composite beams and ECC beams are also proposed. Experimental results show that the proposed formulas are in good agreement with the experimental results, confirming the applicability of various formulas developed. The trend of flexural behavior of composite beams against the reinforcement, ECC and concrete properties has been developed based on a comprehensive parametric study. The following conclusions may be drawn:

- The cracking, yield and ultimate moments of composite beams and ECC beams are higher than these of conventional concrete beams, regardless of the reinforcement used. At the same load, the deflection of composite beams and ECC beams are less than that of conventional concrete beams, having the same amount of reinforcement.
- After yielding of steel reinforcement, the deflections of steel reinforced concrete beams, ECC-concrete composite beams and ECC beams increase even if the load does not increase, while deflections of hybrid reinforced beams increase with the increase of loading.
- For specimens with the same nominal reinforcement ratio converted by elastic modulus ratio, ultimate moment increases with the decrease of nominal reinforcement ratio converted by strength ratio. For specimens with similar nominal reinforcement ratio converted by strength, yield moment decreases with the decrease of nominal reinforcement ratio converted by elastic modulus ratio.
- For the hybrid reinforced concrete beams, the number of cracks increases while the average crack spacing and crack width decrease with increasing the height replacement ratio. The maximum crack width of specimens decrease with the increase of the height replacement ratio, regardless of

the reinforcement used.

- The energy dissipation of reinforced ECC beams is higher than that of reinforced concrete beams and composite beams as the ultimate compressive strain of ECC is higher than that of concrete. Energy dissipation of steel reinforced beams and hybrid reinforced beams are higher than that of FRP reinforced beams.
- For specimens with similar practical reinforcement ratio, the ductility of hybrid reinforced beams is higher than that of reinforced concrete beams. For specimens with the same nominal reinforcement ratio converted by elastic modulus ratio, ductility increases with the increase of nominal reinforcement ratio converted by strength ratio.

Acknowledgement

The authors appreciate the support of the National Natural Science Foundation of China (51678514, 51308490), the Natural Science Foundation of Jiangsu Province, China (BK20130450), Six Talent Peaks Project of Jiangsu Province (JZ-038, 2016), Graduate Practice Innovation Project of Jiangsu Province (SJCX17-0625), the Jiangsu Government Scholarship for Overseas Studies and Top-level Talents Support Project of Yangzhou University.

References

ACI (American Concrete Institute). (2004). "Guide test methods for fiber reinforced polymers (FRPs) for reinforcing or strengthening concrete structures." *ACI 440.3R-04*, Farmington Hills, MI.

Aiello, M. A., & Ombres, L. (2000). "Load-deflection analysis of FRP reinforced concrete flexural members." *J. Compos. Constr.*, 4(4), 164-171.

Aiello, M. A., & Ombres, L. (2002). “Structural performances of concrete beams with hybrid (fiber-reinforced polymer-steel) reinforcements.” *J. Compos. Constr.*, 6(2), 133-140.

Cai, J., Pan, J., & Zhou, X. (2017). “Flexural behavior of basalt FRP reinforced ECC and concrete beams.” *Constr. Build. Mater.*, 142, 423-430.

Chinese National Standard. (2002). “Standard for test method of mechanical properties on ordinary concrete.” *GB/T 50081-2002*, China Building Industry Press, Beijing (in Chinese).

Chinese National Standard. (2010). “Code for design of concrete structures.” *GB 50010-2010*, China Building Industry Press, Beijing (in Chinese).

Ge, W., Zhang, J., Cao, D., & Tu, Y. (2015). “Flexural behaviors of hybrid concrete beams reinforced with BFRP bars and steel bars.” *Constr. Build. Mater.*, 87, 28-37.

Ge, W., Ashour, A. F., Ji, X., Cai, C., & Cao, D. (2018). “Flexural behavior of ECC-concrete composite beams reinforced with steel bars.” *Constr. Build. Mater.*, 159, 175-188.

Grace, N. F., Sayed, G. A., Soliman, A. K., & Saleh, K. R. (1999). “Strengthening reinforced concrete beams using fiber reinforced polymer (FRP) laminates.” *J. ACI Struct.*, 188(8), 865-875.

Gravina, R. J., & Smith, S. T. (2008). “Flexural behaviour of indeterminate concrete beams reinforced with FRP bars.” *Steel Constr.*, 30(9), 2370-2380.

Kara, I. F., Ashour, A. F.& Köroğlu, M. A. (2015). “Flexural behavior of hybrid FRP/steel reinforced concrete beams.” *Compos. Struct.*, 129, 111-121.

Lau, D., & Pam, H. J. (2010). “Experimental study of hybrid FRP reinforced concrete beams.” *Eng. Struct.*, 32(12), 3857-3865.

Leung, H. Y. & Balendran, R. V. (2003). “Flexural behaviour of concrete beams internally reinforced with GFRP rods and steel rebars.” *Struc. Surv.*, 21(4):146-157.

Maalej,M., & Leong, K. S. (2005). “Engineered cementitious composites for effective FRP-strengthening of RC beams.” *Compos. Sci. Technol.*, 65(7), 1120-1128.

Maalej, M., & Li,V. C. (1995).“Introduction of strain hardening engineered cementitious composites in design of reinforced concrete flexural members for improved durability.” *J. ACI Struct.*, 92(2), 167-176.

Maalej, M., Quek, S. T., Ahmed, S. F. U., Zhang, J., Lin, V. W. J., & Leong, K. S. (2012). “Review of potential structural applications of hybrid fiber engineered cementitious composites.” *Constr. Build. Mater.*, 36(11), 216-227.

Masmoudi, R., Thériault, M., &Benmokrane, B. (1998). “Flexural behavior of concrete beams reinforced with deformed fiber reinforced plastic reinforcing rods.” *J. ACI Struct.*, 95(6), 665-676.

Pecce, M., Manfredi, G., & Cosenza, E. (2000). “Experimental response and code models of GFRP RC beams in bending.” *J. Compos. Constr.*, 4(4), 182-190.

Qu, W.,Zhang, X.& Huang, H. (2009). “Flexural behavior of concrete beams reinforced with hybrid (GFRP and steel) bars.” *J. Compos. Constr.*, 13(5), 350-359.

Soric, Z., Kisicek, T., & Galic, J. (2010). “Deflections of concrete beams reinforced with FRP bars.” *Mater. Struct.,* 43(1), 73-90.

Tu, Y., Zhang, J., &Qian, Y. (2009). “Experimental and theoretical investigation of flexural load-carrying capacity of concrete beams reinforced with AFRP tendons.” *J. Southeast Univ. (Nat. Sci.), China*, 39(3), 563-568.

Wang, S., Wu, C., & Li, V. C. (2001). “Tensile strain-hardening behavior of polyvinyl alcohol engineered cementitious composite (PVA-ECC).” *J. ACI Mater.*, 98(6), 483-492.

Xu, S. L., & Li, Q. H. (2009). “Experimental investigation and analysis on flexural performance of functionally graded composite beam crack-controlled by ultrahigh toughness cementitious composites.” *Sci, China Ser, E.*, 52(6), 1648-1664.

Xu, S.,Wang, N. &Li, Q. (2010).“Experimental study on the flexural performance of concrete beam strengthened with ultra high toughness cementitious composites.” *J. Civil. Eng., China*, 43 (5): 17-22.

Xu, Y., & Pan, J. (2013). “Flexural behaviors of double-reinforced ECC beams.” *J. Southeast Univ. (Eng. Ed.), China*, 29(1): 66-72.

Yuan, F., Pan, J., & Leung, C. K. Y. (2013). “Flexural behaviors of ECC and concrete/ECC composite beams reinforced with basalt fiber-reinforced polymer.”*J. Compos. Constr.*, 17(5), 591-602.

Yuan, F., Pan, J. L., & Wu Y. F. (2014). “Numerical study on flexural behaviors of steel reinforced engineered cementitious composite (ECC) and ECC/concrete composite beams.” *Sci. China Technol. Sc.*, 57(3), 637-645.

Zhang, X., Xu, S., & Li, H. (2010). “Theoretical analysis of flexural performance of plain concrete composite beams strengthened with ultrahigh toughness cementitious composite.” *J. Civil Eng., China*, 43(7), 51-62.

Zhang, J., Leung, C. K. Y., & Yin, N. C. (2006). “Flexural performance of layered ECC-concrete composite beam.” *Compos. Sci. Technol.*, 66(11-12), 1501-1512.